Title

CARMIL1-AA selectively inhibits macropinocytosis while sparing autophagy

Journal

Molecular Biology of the Cell, 36(1)

ISSN

1059-1524

Authors

Lim, Rebecca M

Lu, Alexa

Chuang, Brennan M

et al.

Publication Date

2025

DOI

10.1091/mbc.e24-09-0434

Peer reviewed

CARMIL1-AA selectively inhibits macropinocytosis while sparing autophagy

Rebecca M. Lim[1], Alexa Lu[2], Brennan M. Chuang[1], Cecily Anaraki[3], Brandon Chu[1], Christopher J. Halbrook[3,4], and Aimee L. Edinger*[,1,2,4]

[1]Department of Developmental and Cell Biology, Charlie Dunlop School of Biological Sciences, University of California, Irvine, CA 92617; [2]Department of Pharmaceutical Sciences, School of Pharmacy and Pharmaceutical Sciences, University of California, Irvine, CA 92617; [3]Department of Molecular Biology and Biochemistry, Charlie Dunlop School of Biological Sciences, University of California, Irvine, Irvine, CA 92617; [4]Chao Family Comprehensive Cancer Center, University of California, Irvine, Orange, CA 92868

ABSTRACT **Macropinocytosis is reported to fuel tumor growth and drug resistance by allowing cancer cells to scavenge extracellular macromolecules. However, accurately defining the role of macropinocytosis in cancer depends on our ability to selectively block this process. 5-(N-ethyl-N-isopropyl)-amiloride (EIPA) is widely used to inhibit macropinocytosis but affects multiple Na^+/H^+ exchangers (NHE) that regulate cytoplasmic and organellar pH. Consistent with this, we report that EIPA slows proliferation to a greater extent than can be accounted for by macropinocytosis inhibition and triggers conjugation of ATG8 to single membranes (CASM). Knocking down only NHE1 would not avoid macropinocytosis-independent effects on pH. Moreover, contrary to published reports, NHE1 loss did not block macropinocytosis in multiple cell lines. Knocking down CARMIL1 with CRISPR-Cas9 editing limited macropinocytosis, but only by 50%. In contrast, expressing the CARMIL1-AA mutant inhibits macropinocytosis induced by a wide range of macropinocytic stimuli to a similar extent as EIPA. CARMIL1-AA expression did not inhibit proliferation, highlighting the shortcomings of EIPA as a macropinocytosis inhibitor. Importantly, autophagy, another actin dependent, nutrient-producing process, was not affected by CARMIL1-AA expression. In sum, constitutive or inducible CARMIL1-AA expression reduced macropinocytosis without affecting proliferation, RAC activation, or autophagy, other processes that drive tumor initiation and progression.**

SIGNIFICANCE STATEMENT

- Lack of a specific inhibition strategy limits our ability to accurately define the contribution of macropinocytosis to biological processes, including tumor initiation and progression.
- Using cancer cell lines, the authors demonstrate that common inhibition strategies, the NHE inhibitor EIPA or NHE1 knockdown, have profound macropinocytosis-independent effects on proliferation, trigger noncanonical LC3-II lipidation, and/or fail to inhibit macropinocytosis. In contrast, the CARMIL1-AA mutant blocks macropinocytosis without inhibiting proliferation, membrane ruffling, or autophagy.
- These findings suggest that CARMIL1-AA overexpression can be used to separate the contributions that autophagy and macropinocytosis make to tumor progression and drug resistance.

Monitoring Editor
Sergio Grinstein
Hospital for Sick Children

Received: Oct 1, 2024
Revised: Nov 15, 2024
Accepted: Nov 19, 2024

Challenge

Cross-Validation

New Hypothesis

INTRODUCTION

Macropinocytosis allows nonselective bulk uptake of exosomes, extracellular matrix proteins, albumin, and dead cell debris (Finicle *et al.*, 2018). This endocytic process is stimulated by the activation of Ras, PI3K, receptor tyrosine kinases, Wnt, and Src signaling pathways (Amyere *et al.*, 2000; Commisso *et al.*, 2013; Palm *et al.*, 2017; Tajiri *et al.*, 2017; Kim *et al.*, 2018; Redelman-Sidi *et al.*, 2018; Hodakoski *et al.*, 2019; Jayashankar and Edinger, 2020). A wide variety of cancer cells including glioblastoma, pancreas, lung, prostate, breast, colorectal, and bladder cancer cells scavenge nutrients from macropinocytosed macromolecules. Given that inadequate vasculature limits the delivery of blood borne nutrients to tumor cells, this scavenging process could be an important contributor to tumor cell growth and survival, particularly in the presence of chemotherapies that target anabolic pathways or that increase the demand for biosynthesis (Jayashankar and Edinger, 2020). 5-(N-ethyl-N-isopropyl)-amiloride (EIPA), a chemical inhibitor of multiple sodium/hydrogen exchanger (NHE) isoforms (Masereel, 2003), has been widely used to define the role of macropinocytosis in tumor progression (Bar-Sagi and Feramisco, 1986; Ridley *et al.*, 1992; Araki *et al.*, 1996, 2007; West *et al.*, 2000; Kabayama *et al.*, 2011; Fujii *et al.*, 2013; Hoeller *et al.*, 2013; Nonnenmacher *et al.*, 2015; Kim *et al.*, 2018; Sedlyarov *et al.*, 2018; Ramirez *et al.*, 2019; Maxson *et al.*, 2021). However, EIPA inhibits RAC and macropinocytosis indirectly by modulating submembranous pH (Koivusalo *et al.*, 2010); NHE proteins control cytosolic and organellar pH (Slepkov *et al.*, 2007; Cheng *et al.*, 2019). By inhibiting proton transport, EIPA would also affect cellular metabolism, signal transduction, and protein conformation, processes that impact tumor growth (Steffan *et al.*, 2009; Orij *et al.*, 2011; Isom *et al.*, 2013; Ko *et al.*, 2020; Rolver *et al.*, 2020; Jin *et al.*, 2022; Okreglak *et al.*, 2023). EIPA is selective for macropinocytosis among endocytic processes, making it a useful tool to determine the background in the 70 kD dextran uptake assays used to measure macropinocytosis (Kim *et al.*, 2018). However, a more selective inhibitor is needed to accurately define the potential therapeutic value of targeting macropinocytosis in tumors.

Macropinosome formation requires actin cytoskeleton remodeling. CARMIL1 (capping protein interaction (CPI)-containing, Arp2/3, myosin 1-linker 1) regulates actin capping protein activity, thereby promoting lamellipodia and macropinosome formation (Edwards *et al.*, 2013; Zwolak *et al.*, 2013). The KR987/989AA double-point mutation within the CPI region of CARMIL1 (CARMIL1-AA) disrupts the interaction with actin capping protein; this mutant cannot support macropinocytosis (Edwards *et al.*, 2013). Surprisingly, although macropinosomes no longer form, CARMIL1-AA supports normal RAC GTPase activation and cell migration in HT1080 fibrosarcoma cells, most likely because these functions do not depend on CARMIL1 binding to capping protein. Previously, we have shown that replacing the endogenous protein with CARMIL1-AA inhibits macropinocytosis in 4T1 mammary cancer cells without affecting cellular proliferation in nutrient replete medium (Jayashankar and Edinger, 2020). However, whether CARMIL1-AA also impacts autophagy, an important actin-dependent survival mechanism under nutrient stress, has not been assessed.

While macropinocytosis provides exogenous nutrients that can be used to build biomass, autophagy protects cells from nutrient stress by recycling cell-intrinsic macromolecules so that their building blocks can be used to support essential processes (Kaizuka *et al.*, 2016; Florey and Overholtzer, 2019). Through autophagy, nonessential cellular components are encapsulated in LC3-II–marked vesicles that eventually fuse with lysosomes, leading to degradation of their contents and the release of recycled building blocks that can be directed to ATP production or biosynthesis. In addition, autophagy supports tumor growth by limiting antitumor immunity and by promoting drug resistance and the secretion of amino acids, growth and angiogenic factors, inflammatory cytokines, and extracellular matrix components (Zhang *et al.*, 2017; Chavez-de Souza *et al.*, 2020; Dominguez *et al.*, 2020; Li *et al.*, 2020; Yamamoto *et al.*, 2020; Actis *et al.*, 2021; Debnath *et al.*, 2023). The actin cytoskeleton plays a critical role in autophagosome formation, trafficking, and fusion with lysosomes (Kast and Dominguez, 2017; Dong and Quan, 2024). Accordingly, while a therapeutic that blocks both macropinocytosis and autophagy may be particularly effective, dissecting the role of macropinocytosis in tumorigenesis requires a strategy that can block macropinocytosis while leaving autophagy intact. Here we show that, while EIPA has multiple macropinocytosis-independent effects and NHE1 knockdown fails to inhibit macropinocytosis, CARMIL1-AA expression blocks macropinocytosis without impacting proliferation, RAC activation, or autophagic flux.

RESULTS

EIPA affects more than macropinocytosis

As mentioned above, EIPA inhibits macropinocytosis by inactivating NHE proteins that control cytosolic and organellar pH (Masereel, 2003; Slepkov *et al.*, 2007; Koivusalo *et al.*, 2010; Cheng *et al.*, 2019). The minimal concentration of EIPA required to inhibit macropinocytosis was determined in two cancer cell lines, PyMT mouse mammary carcinoma cells and HeLa human cervical carcinoma cells. Both cell lines are contextually macropinocytic, exhibiting basally low levels of macropinocytosis until they are stressed or stimulated. Similar to multiple normal and transformed cell types (Kim *et al.*, 2018; Jayashankar and Edinger, 2020; Zhang *et al.*, 2021), nutrient stress increased macropinocytosis in PyMT cells as measured by 70 kD dextran uptake (Figure 1, A and B). Although 10, 20, and 50 μM EIPA partially blocked this increase in dextran uptake, 75 μM EIPA was required to maximally suppress macropinocytosis (Figure 1, C and D). Because the dextran index in nutrient-stressed PyMT cells treated with 75 μM EIPA is lower than that of control PyMT cells maintained in nutrient-replete medium, PyMT cells are weakly macropinocytic in the absence of nutrient stress.

This article was published online ahead of print in MBoC in Press (http://www.molbiolcell.org/cgi/doi/10.1091/mbc.E24-09-0434) on November 27, 2024.

Author Contributions: R.M.L., C.A., B.C., and A.L.E. conceived and designed the experiments; R.M.L., A.L., and B.C. performed the experiments; R.M.L., B.C., and C.A. analyzed the data; R.M.L. and A.L.E. drafted the article; R.M.L. prepared the digital images; C.J.H. supervision, reviewed and edited manuscript, funding acquisition; A.L.E. supervision and Funding Acquisition.

Conflict of interest: The authors declare no financial conflicts of interest.

*Address correspondence to: Aimee Edinger (aedinger@uci.edu).

Abbreviations used: EIPA5-(N-ethyl-N-isopropyl)-amiloride; NHEsodium/hydrogen exchangers; CASMconjugation of ATG8 to single membranes; CFSEcarboxyfluorescein succinimidyl ester; CPIcapping protein interaction; CARMIL1containing, Arp2/3, myosin 1-linker 1; BafA1bafilomycin A1; HBSS, 5-(N-ethyl-N-isopropyl)-amiloride; NHEsodium/hydrogen exchangers; CASMconjugation of ATG8 to single membranes; CFSEcarboxyfluorescein succinimidyl ester; CPIcapping protein interaction; CARMIL1containing, Arp2/3, myosin 1-linker 1; BafA1bafilomycin A1; HBSSHank's buffered salt solution

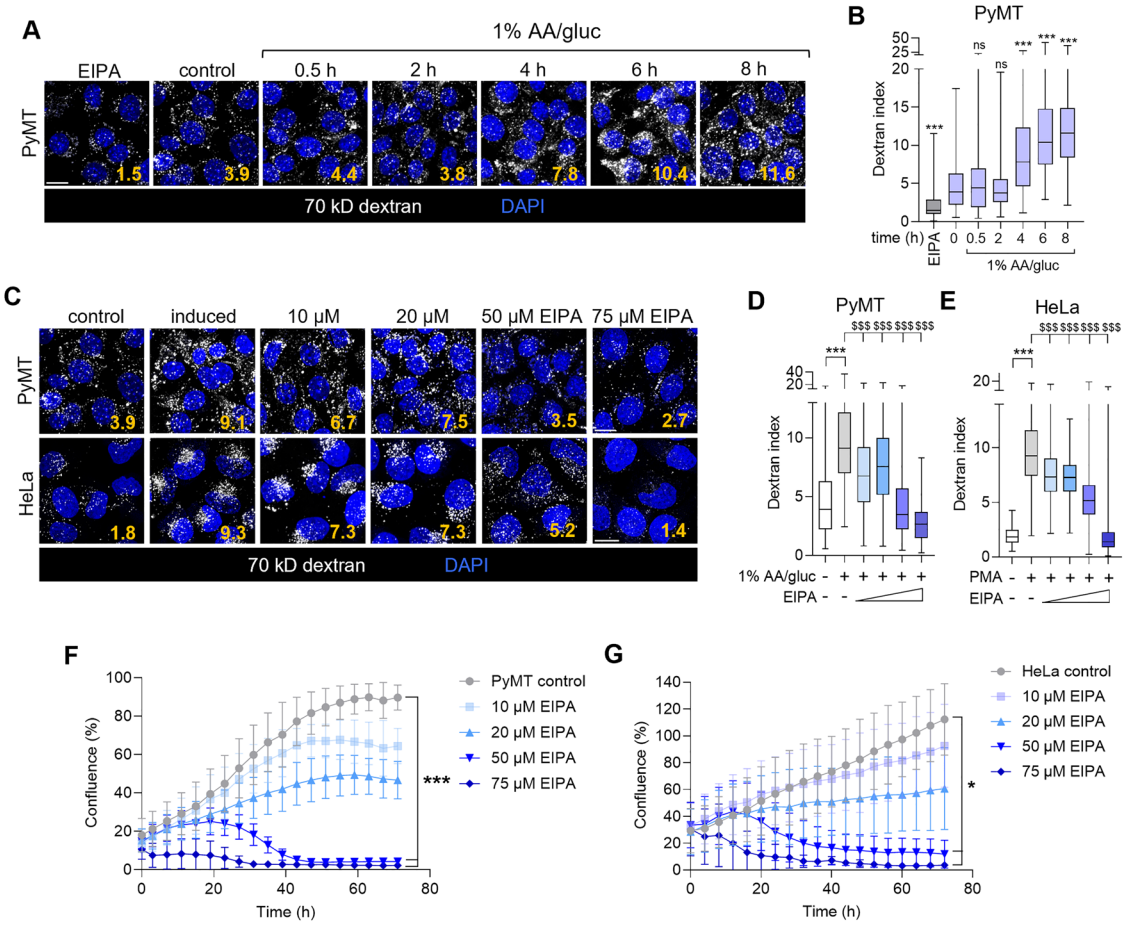

FIGURE 1: EIPA is not a selective macropinocytosis inhibitor. (A, B) 70 kD dextran uptake analysis in PyMT cells incubated in complete media (control or 0 h timepoint) or 1% AA/gluc media for the indicated interval. PyMT cells maintained in 1% AA/gluc media for 6 h were additionally treated with 75 μM EIPA for 1.5 h. (C–E) PyMT and HeLa cells were either incubated in complete media (control) or induced with 1% AA/gluc for 6 h (PyMT cells) or with 250 nM PMA for 30 min (HeLa cells). Where indicated, cells were treated with the indicated concentrations of EIPA. Numbers in images represent the median dextran index, box and whisker plots show the median and quartiles. At least 100 cells from each of two biological replicates were analyzed. Scale bars, 20 μm. (F, G) Cellular proliferation in PyMT (F) or HeLa (G) cells in complete medium in the presence or absence of EIPA as measured by the Biospa platform. Mean ± SD shown from three biological replicates. In B, D, and E, statistical significance was determined using a one-way ANOVA with Dunn's post-hoc analysis to correct for multiple comparisons. In B, ***$p<0.001$, ns = not significant $p>0.05$ comparing the 0 h nutrient stress timepoint for all conditions. In D and E, ***$p<0.001$ comparing stimulated PyMT and HeLa cells to unstimulated control cells, $$$$p<0.001$ comparing EIPA-treated PyMT and HeLa cells to the stimulated cells treated with vehicle. In F and G, statistical significance was determined using a one-way ANOVA with Tukey's post-hoc analysis to correct for multiple comparisons; ***$p<0.001$ and *$p<0.05$ comparing the confluence of PyMT and HeLa control cells with cells treated with 50 or 75 μM EIPA.

Notably, 50 μM EIPA reduces dextran uptake to the extent that matches PyMT cells growing in complete medium. Macropinocytosis can be induced in HeLa cervical carcinoma cells with phorbol 12-myristate 13-acetate (PMA, Figure 1, C and E). PMA activates PKC isoforms resulting in the induction of macropinocytosis in macrophages and other cell types including HeLa cells (Swanson, 1989; Tisdale *et al.*, 2014). Similar to nutrient stressed PyMT cells, 75 μM EIPA was required to maximally inhibit PMA-stimulated macropinocytosis in HeLa cells. Because the dextran index in unstimulated HeLa cells and in HeLa cells treated with PMA and 75 μM EIPA was similar, HeLa cells are minimally macropinocytic in the absence of stimulation. In sum, Figure 1, A–E show that 50 or 75 μM EIPA, respectively, reduces the rate of macropinocytosis to the levels seen in control, unstimulated PyMT or HeLa cells.

Because EIPA targets multiple NHE isoforms, it would be expected to have macropinocytosis-independent effects on cancer cell proliferation and survival (Masereel, 2003; Koivusalo *et al.*, 2010; Jayashankar and Edinger, 2020; Rolver *et al.*, 2020; Inoue *et al.*, 2021). To test this experimentally, we measured cell proliferation in the presence and absence of EIPA under conditions where macropinocytosis was unlikely to play a major role supporting cellular bioenergetics: weakly macropinocytic PyMT and HeLa cells maintained in nutrient replete medium that lacks macropinocytic fuel (not supplemented with additional albumin, ECM protein, or necrotic debris). In both PyMT and HeLa cells, 50 or 75 μM EIPA dramatically reduced proliferation and viability relative to the control over the course of 24 h (Figure 1, C, D, and F). Taken together, these experiments strongly suggest that EIPA reduces cancer cell proliferation and survival to a greater extent than can be explained

by macropinocytosis inhibition alone. We therefore sought to identify a more selective means to inhibit macropinocytosis and isolate its contribution to cancer biology.

NHE-1 inhibition is not sufficient to phenocopy the effects of EIPA on macropinocytosis

NHE1 knockdown has been reported to inhibit macropinocytosis in KRAS-mutant pancreatic cancer cells and in myeloid cells (Su *et al.*, 2021; Lin *et al.*, 2022). Inhibiting only NHE1 might be a more selective macropinocytosis inhibition strategy than EIPA. However, neither study quantified the direct effect of NHE1 knockdown on macropinosome formation via 70 kD dextran uptake or using live imaging, the standard assays in the field. To establish whether NHE1 loss could provide a more selective approach to inhibiting macropinocytosis across cancer classes, NHE1 levels were reduced via CRISPR-Cas9 genomic editing in both contextually macropinocytic HeLa cells and constitutively macropinocytic MDA-MB-231 human breast cancer cells that carry the $KRAS^{G13D}$ mutation (Kozma *et al.*, 1987; Jayashankar and Edinger, 2020). The CRISPR editing plasmids were introduced by transient transfection to avoid the long-term negative effects of constitutive Cas9 expression. Efficient NHE1 knockdown was achieved with two different single-guide RNAs (sgRNAs) in multiple clones obtained from both cell lines (Figure 2, A–D). However, NHE1 loss did not significantly reduce 70 kD dextran uptake in PMA-stimulated HeLa or unstimulated MDA-MB-231 cells when compared with wild type or empty vector controls (Figure 2, E–H). Moreover, EIPA still efficiently inhibited macropinocytosis in cells lacking NHE1, illustrating that NHE1 loss is not sufficient to recapitulate the effects of EIPA at least in the cell lines studied. The reduced responsiveness of some NHE1 knockdown clones to EIPA (e.g., HeLa clones 1-2 and 2-1 and MDA-MB-231 clone 1-2) was reproduced in independent experiments and may reflect the up-regulation of other NHE isoforms as part of an adaptive response to the constitutive loss of NHE1. These results indicate that NHE1 knockdown is not sufficient to inhibit macropinocytosis and suggest that biological effects linked to NHE1 knockdown (Su *et al.*, 2021; Lin *et al.*, 2022) may be pH-dependent rather than macropinocytosis-dependent.

The CARMIL1-AA mutant inhibits macropinocytosis

CARMIL1, a regulator of actin capping protein, is essential for membrane ruffling and macropinocytosis in the HT1080 fibrosarcoma cell line that carries an activating mutation in NRAS (Edwards *et al.*, 2013). To determine whether CARMIL1 is also essential for macropinocytosis in PyMT and HeLa cells, CARMIL1 was knocked down using CRISPR-Cas9 genomic editing. CARMIL1 protein levels were reduced by 80–90% in edited clones from both cell lines (Figure 3, A–D). Constitutive knockdown of endogenous CARMIL1 was well-tolerated in both PyMT and HeLa cell clones, consistent with CARMIL1 dependency scores in the DepMap portal clustered around zero (Tsherniak *et al.*, 2017). As expected, CARMIL1 knockdown significantly but incompletely inhibited macropinocytosis in both nutrient-stressed PyMT and PMA-stimulated HeLa cells (Figure 3, E–H). If the level of dextran uptake in EIPA-treated cells is considered as background, CARMIL1 knockdown reduced the dextran index in PyMT cells by ~75% and in HeLa cells by ~50%. Dextran uptake results were confirmed by live-cell imaging. PyMT CARMIL1 knockdown clones exhibited significantly reduced membrane ruffling and very limited macropinosome formation under nutrient stress, similar to EIPA-treated cells (Supplemental Videos S1–S3; Figure 3I). Collectively, these results show that CARMIL1 is required for optimal membrane ruffling and macropinosome formation in PyMT and HeLa cells and that knocking down CARMIL1 does not limit macropinocytosis as effectively as EIPA.

Alanine mutations in two residues (KR987/989AA) within the CPI-domain of CARMIL1 required for actin capping protein binding produces a form of CARMIL1 that supports membrane ruffling, migration, and RAC activation but not macropinocytosis in HT1080 cells lacking endogenous CARMIL1 (Hernandez-Valladares *et al.*, 2010; Edwards *et al.*, 2013). While reconstitution with wild type CARMIL1 restored macropinocytosis (Figure 4, A–D), dextran uptake was not significantly increased in CARMIL1 knockdown cells reconstituted with CARMIL1-AA. Importantly, neither CARMIL1 knockdown (Figure 3) nor CARMIL1 knockdown followed by reconstitution with CARMIL1-AA (Figure 4, A–D) inhibited macropinocytosis as well as EIPA. Because CARMIL1 functions as a homodimer (Zwolak *et al.*, 2013; Wang *et al.*, 2016), whether the CARMIL1-AA mutant could function as a dominant-negative mutant was also tested. CARMIL1-WT or CARMIL1-AA was constitutively expressed in control PyMT cells without first knocking down endogenous CARMIL1 and paired, clonal cell lines with matched levels of total CARMIL1 protein (2- to 4-fold above control levels) were selected (Figure 4, E and F). Consistent with function as a dominant-negative mutant, CARMIL1-AA inhibited dextran uptake even in the presence of endogenous CARMIL1 while CARMIL1-WT overexpression did not affect dextran uptake (Figure 4, G and H). Interestingly, macropinocytosis inhibition by CARMIL1-AA was more efficient in the presence of endogenous CARMIL1 (Figure 4, E–H) than its absence (Figure 4, A–D). These results show that CARMIL1-AA expression inhibits macropinocytosis to a similar extent as EIPA and has the potential to be more selective.

To complement dextran uptake assays, necrocytosis was also examined in CARMIL1-WT and -AA clones where endogenous CARMIL1 is still expressed. Necrocytosis, the scavenging of nutrients from necrotic cell debris via macropinocytosis, protects cancer cells from death induced by the topoisomerase inhibitor doxorubicin, a therapeutic that increases demand for nucleotide synthesis to support DNA repair (Brown *et al.*, 2017; Jayashankar and Edinger, 2020). Fluorescent necrotic cell debris was produced without the addition of toxic chemicals by subjecting carboxyfluorescein succinimidyl ester (CFSE)-labeled FL5.12 cells to both nutrient and IL-3 withdrawal at high density (200 million cells/ml). FL5.12 murine hematopoietic cells are dependent on IL-3 for proliferation and survival (Edinger and Thompson, 2002). Fluorescent apoptotic cells were produced by short-term IL-3 deprivation of CFSE labeled FL5.12 cells maintained at a lower density (1 million cells/ml) (Figure 5A). As expected, necrotic cell debris, but not apoptotic cells, could be consumed by CARMIL1-WT overexpressing PyMT cells (Figure 5, B–D). CARMIL1-AA–expressing PyMT cells could not take up necrotic cell debris, consistent with the loss of macropinocytosis. In keeping with the results of these uptake assays, necrotic cell debris protected CARMIL1-WT–expressing PyMT cells from doxorubicin while CARMIL1-AA–overexpressing cells remained sensitive (Figure 5, E–G). CARMIL1-WT cells displayed a slight survival advantage even in the absence of exogenous necrotic debris, suggesting that debris from PyMT cells that succumbed to doxorubicin was scavenged by neighboring macropinocytic cells. These results show that CARMIL1-AA expression is sufficient to block macropinocytosis in PyMT cells even in the presence of endogenous CARMIL1.

Several additional experiments were conducted to confirm that CARMIIL1-AA could function as a dominant negative mutant. Live-cell imaging indicated that while CARMIL1-WT overexpression was without apparent effect, CARMIL1-AA–expressing PyMT cells

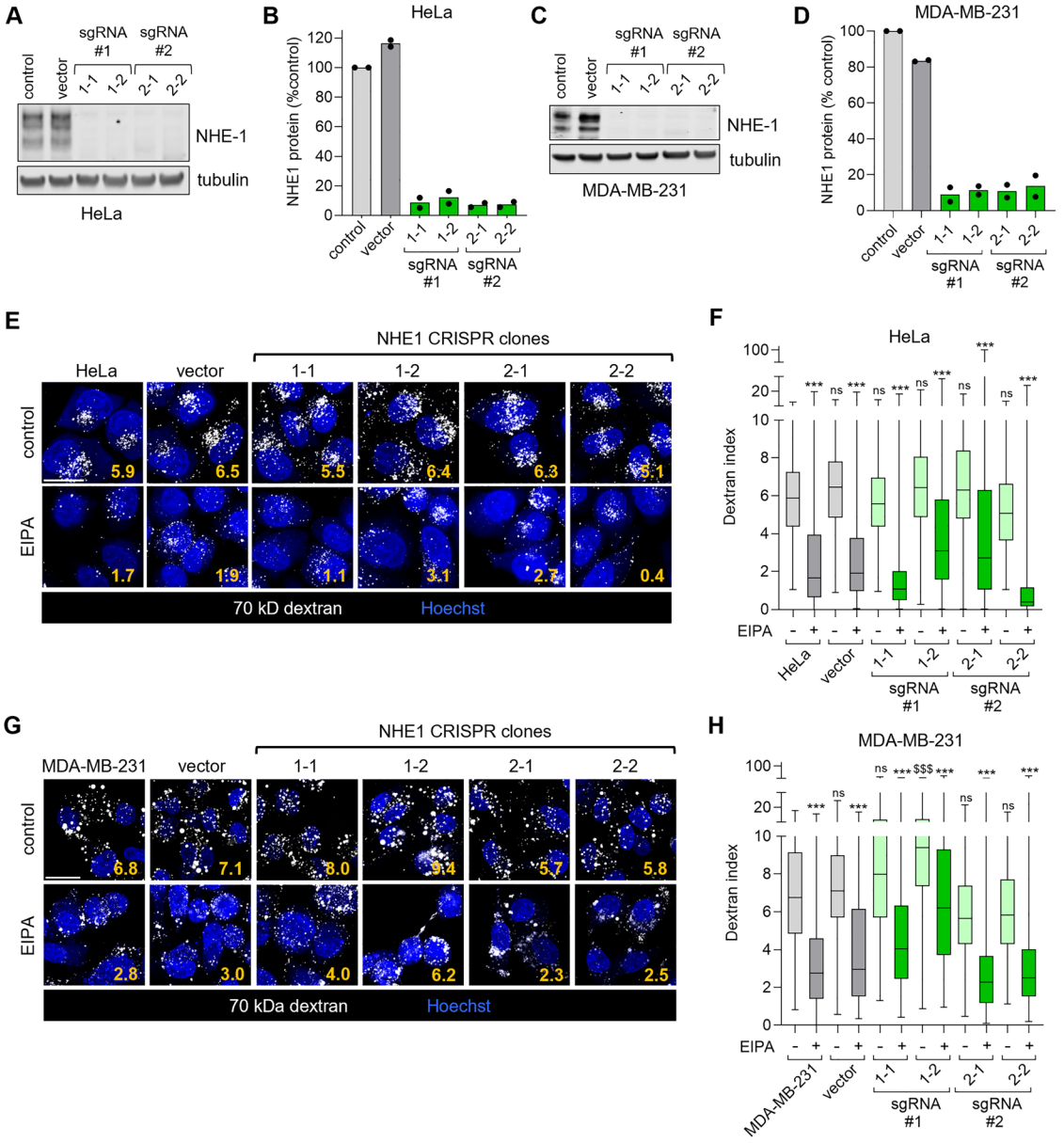

FIGURE 2: NHE-1 loss does not recapitulate the effect of EIPA on macropinocytosis. (A–D) Validation of HeLa (A, B) or MDA-MB-231 (C, D) NHE-1 CRISPR/Cas9 knockdown clones. Two different clones generated with two different sgRNAs are shown; quantified results were first normalized to tubulin and then to the untreated control. Two independent Western blots were quantified with similar results. (E–H) Dextran uptake analysis in control and NHE-1 knockdown clones. HeLa cells (E, F) were stimulated with 250 nM PMA to induce macropinocytosis; MDA-MB-231 cells (G, H) were left unstimulated. Cells were incubated with 1 mg/ml dextran for 30 min ± 75 μM EIPA (1 h pre-treatment). The numbers on images represent the median dextran index calculated from >100 cells analyzed from each of two biological replicates conducted on different days. Box and whisker plots show medians and quartiles. Scale bar, 20 μm. In F and H, statistical significance was calculated using a one-way ANOVA with Dunn's post-hoc analysis to correct for multiple comparisons. ***$p<0.001$ comparing each HeLa and MDA-MB-231 clonal cell line to the control sample treated with 75 μM EIPA; \$\$\$$p<0.001$, ns (not significant, $p>0.05$) comparing each HeLa and MDA-MB-231 NHE-1 knockdown or vector clone without EIPA to the untransduced cells without EIPA.

exhibited membrane ruffling but no macropinosome formation even in the presence of endogenous CARMIL1 (Supplemental Videos S4 and S5; Figure 3I). Moreover, subsequent CRISPR-mediated knockdown of endogenous CARMIL1 in the CARMIL1-AA PyMT clones using an sgRNA targeting an intron-exon junction that is not present in the cDNA did not further reduce macropinocytosis and may have even triggered compensatory changes in gene expression that partially restored macropinocytosis (Supplemental Figure S1, A–D). To confirm that reduced macropinocytosis in CARMIL1-AA–expressing clones was not a result of clonal heterogeneity, PyMT clones with doxycycline-inducible CARMIL1-AA or CARMIL1-WT expression were generated. In both the transduced, drug selected population and in clonal cell lines derived from this population, induction of CARMIL1-AA expression with doxycycline

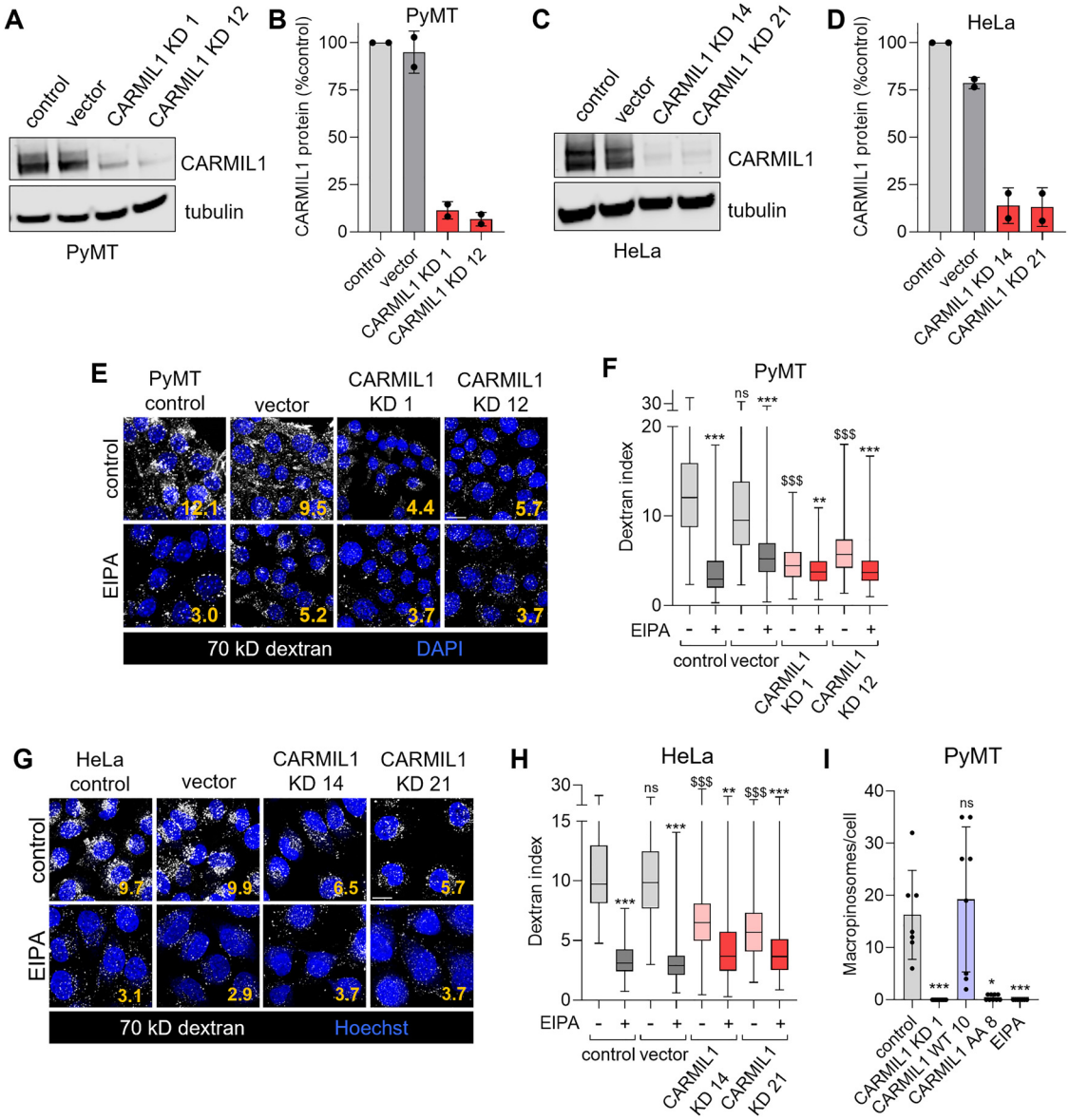

FIGURE 3: CARMIL1 supports macropinocytosis in PyMT and HeLa cells. A–D, Validation of PyMT (A, B) and HeLa (C, D) CARMIL1 CRISPR/Cas9 knockdown clones. Two different clones are shown; quantified results were first normalized to tubulin and then to the untreated control. Two independent western blots were quantified with similar results. (E–H) Dextran uptake analysis in control and CARMIL1 knockdown clones. PyMT cells (E, F) were stimulated with 1% AA/gluc media for 6 h to induce macropinocytosis while HeLa cells (G, H) were stimulated with 250 nM PMA for 0.5 h. Cells were incubated with 1 mg/ml dextran for 30 min ± 75 μM EIPA. The numbers on images represent the median dextran index calculated from >100 cells analyzed from each of two biological replicates conducted on different days; box and whisker plots show median and quartiles. Scale bar, 20 μm. (I) Number of macropinosomes formed per cell over 2 h from live-cell imaging (Supplemental Videos S1–S5). Data were collected from three independent videos per condition, each dot represents one cell. In F, H, and I, statistical significance was calculated using a one-way ANOVA with Dunn's or Tukey's post-hoc analysis to correct for multiple comparisons. In F and H, $^{**}p<0.01$ and $^{***}p<0.001$ comparing each PyMT and HeLa clonal cell line with and without EIPA addition; $\$\$\$p<0.001$, ns (not significant, $p>0.05$) comparing each PyMT and HeLa clonal cell line to control PyMT and HeLa cells each without EIPA. In I, $^{*}p<0.05$, $^{***}p<0.001$, ns (not significant, $p>0.05$) comparing each sample to the control, untransduced PyMT cells.

reduced dextran uptake to a similar extent as EIPA despite the presence of endogenous CARMIL1 protein (Supplemental Figure S2, A–H). Induction of CARMIL1-WT with doxycycline did not affect macropinocytosis. Finally, the ability of CARMIL1-AA expression to reduce macropinocytosis in HeLa cells in the presence of endogenous CARMIL1 was evaluated. Comparing CARMIL1-WT 16 and -AA 13 HeLa clones matched for expression levels, the CARMIL1-AA mutant inhibited macropinocytosis stimulated by PMA, EGF, or Wnt3a (Figure 6, A–H). Taken together, these results indicate that CARMIL1-AA overexpression can inhibit macropinocytosis stimulated by nutrient stress, PMA, or cytokines to a similar extent as EIPA without the need for knockdown of the endogenous protein.

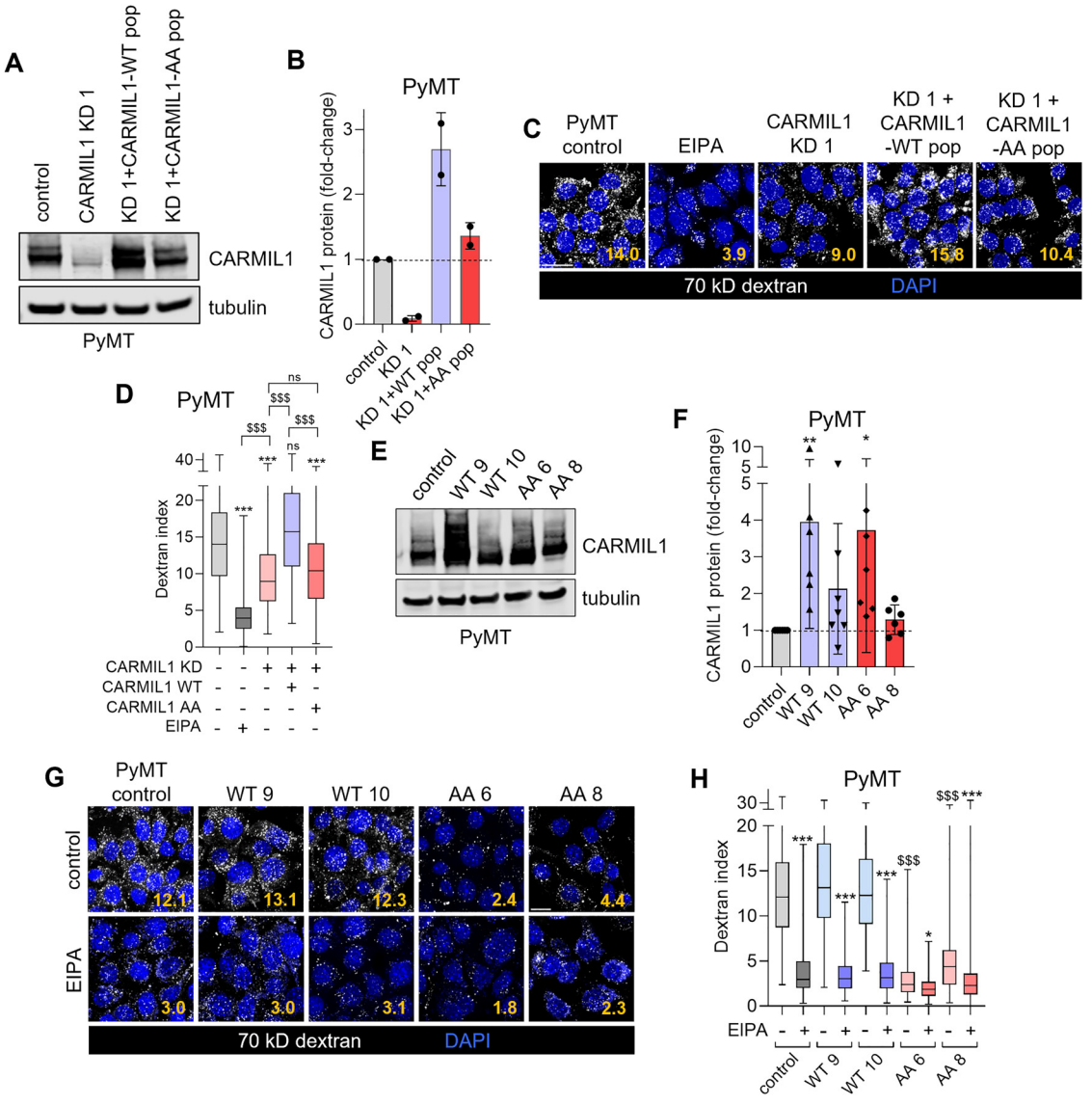

FIGURE 4: CARMIL1-AA is a more effective inhibitor of macropinocytosis in the presence of endogenous CARMIL1. (A, B) Validation of CARMIL1-WT or CARMIL1-AA reconstitution in CARMIL1 knockdown PyMT cells; cell populations are shown. Quantified results were first normalized to tubulin and then to the untreated control. Two independent Western blots were quantified with similar results. (C, D) Dextran uptake analysis in the cells in A and B. (E, F) Validation of CARMIL1-WT or CARMIL1-AA expression in PyMT clonal cell lines where endogenous CARMIL1 is still expressed. Two different clones of CARMIL1-WT and CARMIL1-AA are shown; quantified results were first normalized to tubulin and then to the untreated control. Six to seven independent Western blots were quantified with similar results. (G, H) Dextran uptake analysis in PyMT clones in E and F. For all dextran assays (C,D,G,H), PyMT cells were stimulated with 1% AA/gluc media for 6 h, 75 μM EIPA was added where indicated. The numbers on images represent the median dextran index calculated from >100 cells analyzed from each of 2 biological replicates conducted on different days; box and whisker plots show median and quartiles. Scale bar, 20 μm. In D and H, statistical significance was calculated using a one-way ANOVA with Dunn's post-hoc analysis to correct for multiple comparisons. In D, ***$p<0.001$, ns (not significant, $p>0.05$) comparing to control untransduced PyMT cells; \$\$\$$p<0.001$, ns (not significant, $p>0.05$) comparing the indicated samples. In H, *$p<0.05$, ***$p<0.001$ comparing each clonal cell line ± EIPA; \$\$\$$p<0.001$ compared with the control untransduced PyMT cells without EIPA. In F, statistical significance was calculated using a one-way ANOVA with Tukey's post-hoc analysis to correct for multiple comparisons; *$p<0.05$, **$p<0.01$ comparing each overexpressing CARMIL1-WT or -AA clone to the control untransduced PyMT cells.

CARMIL1-AA does not interfere with cellular proliferation, migration, or RAC activation

PyMT and HeLa cell clones with matched CARMIL1-WT or -AA expression levels proliferated at the same rate as the parental cell lines in complete medium (Figure 7, A and B), similar to the results reported in 4T1 cells with CARMIL1 knockdown and CARMIL1-AA expression (Jayashankar and Edinger, 2020). The observation that non-macropinocytic CARMIL1-AA cells proliferated at the same rate as macropinocytosis-competent CARMIL1-WT cells in complete medium confirms that the profound effect of EIPA on

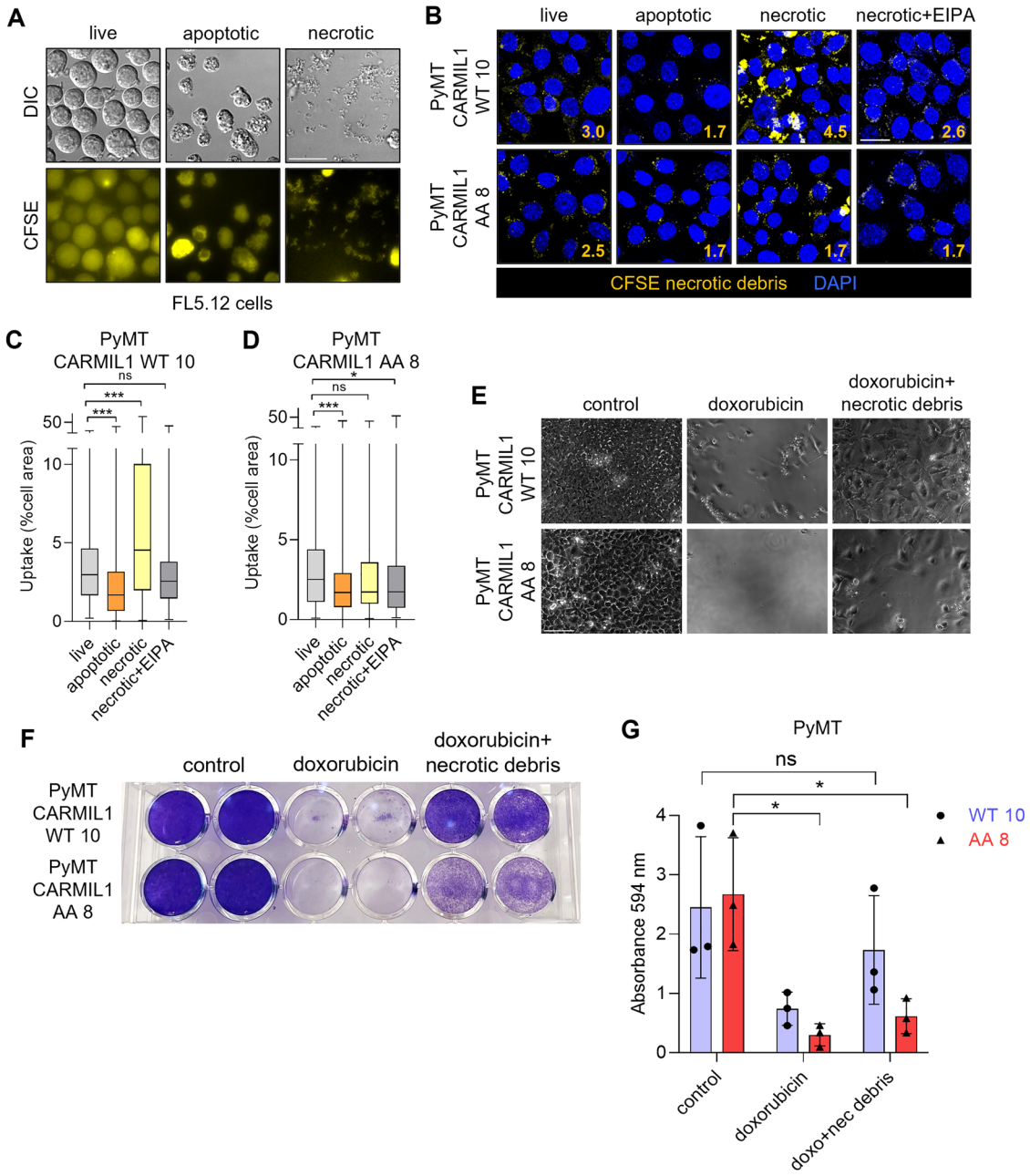

FIGURE 5: CARMIL1-AA hinders necrotic uptake and drug resistance in PyMT cells. (A) CFSE-labeled FL5.12 live, apoptotic, or necrotic cells by DIC brightfield and fluorescent imaging. Scale bar, 20 μm. (B–D) Uptake of CFSE-labeled live, apoptotic, or necrotic cells by PyMT CARMIL1-WT 10 or CARMIL1-AA 8 overexpressing cells pretreated with 1% AA/gluc media for 6 h. The numbers on images represent the median necrotic uptake index calculated from >100 cells analyzed from each of two biological replicates conducted on different days. Scale bar, 20 μm. (E–G) PyMT CARMIL1-WT or -AA clonal cell lines were treated ± 1 μM doxorubicin with or without addition of 10 million cell units of necrotic debris in complete media for 72 h. Widefield images (E) taken prior to fixation and staining (F) and quantification (G) with crystal violet. In (C, D) statistical significance was calculated using a one-way ANOVA with Dunn's post-hoc analysis to correct for multiple comparisons. *$p<0.05$, ***$p<0.001$, ns (not significant, $p>0.05$) for the comparisons shown. In G, statistical significance was calculated using a two-way ANOVA with Tukey's post-hoc analysis to correct for multiple comparisons. *$p<0.05$, ns (not significant, $p>0.05$) for the comparisons shown.

proliferation in nutrient replete medium (Figure 1, F and G) is unrelated to macropinocytosis inhibition. In NRAS-mutant HT1080 fibrosarcoma cells with CARMIL1 knockdown, CARMIL1-AA supported cellular migration and RAC GTPase activation (Edwards *et al.*, 2013). Consistent with this, CARMIL1-AA expression did not interfere with migration in PyMT cells. In a scratch assay, PyMT clones expressing CARMIL1-WT or -AA closed the wound with similar kinetics to control cells (Figure 7, C and D). HeLa cells were more sensitive to mitomycin C (used to block proliferation) at the standard concentration of 10 μg/ml than PyMT cells, but

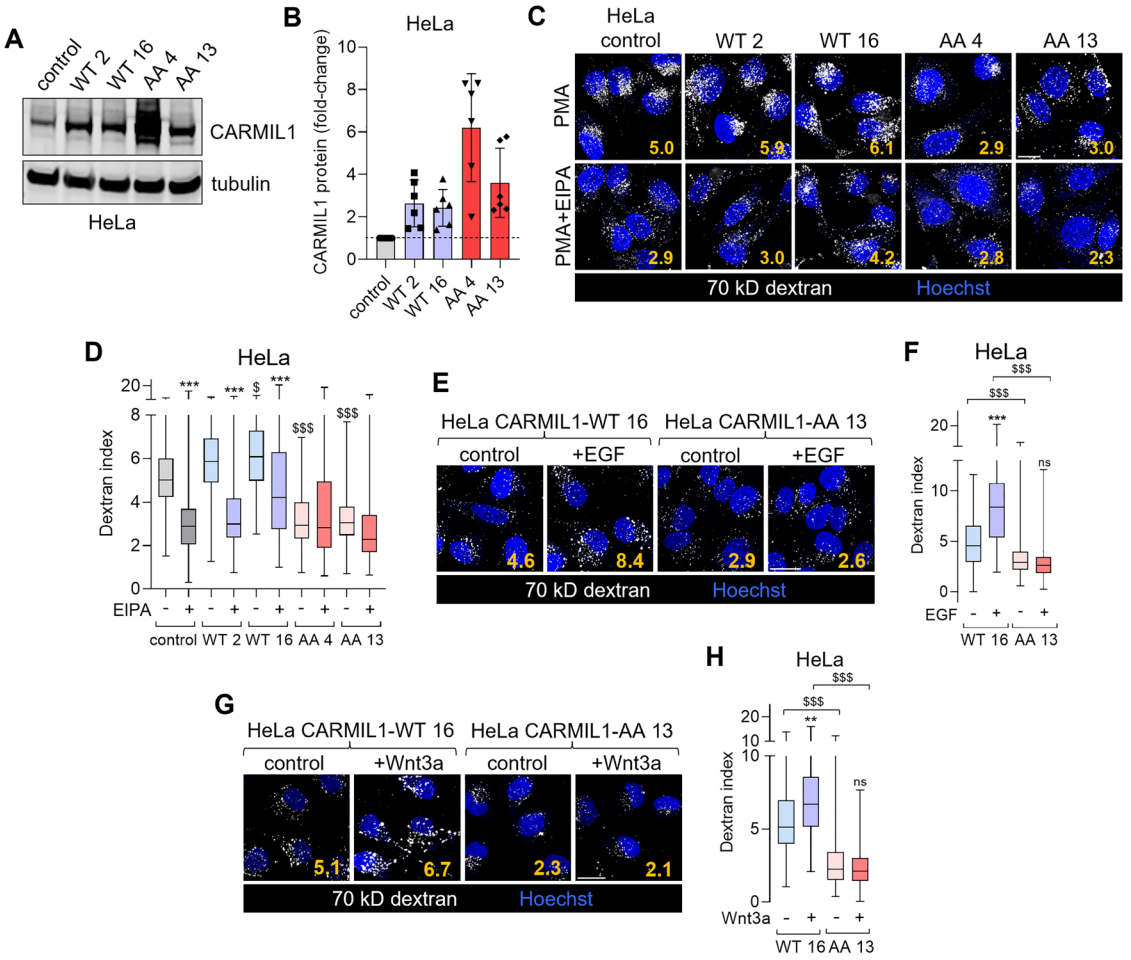

FIGURE 6: CARMIL1-AA inhibits macropinocytosis in HeLa cells. (A, B) Validation of CARMIL1-WT and CARMIL1-AA expression in HeLa cells. Two different CARMIL1-WT and CARMIL1-AA clones are shown; CARMIL1 level was first normalized to tubulin and then to the untreated control. Five to six independent Western blots were quantified with similar results. (C–H) Dextran analysis of HeLa CARMIL1-WT and CARMIL1-AA expressing clones stimulated with 250 nM PMA (C, D), 100 ng/ml EGF (E, F), or 100 ng/mL Wnt3a (G, H) ± 75 μM EIPA (1 h pretreatment). For E and F, HeLa cells were serum starved for 16 h before stimulation with 100 ng/ml EGF and addition of dextran. For G and H, HeLa cells were serum starved for 6 h and treated with 20 μg/ml cycloheximide for the last 4 h of incubation before stimulation with Wnt3a and addition of dextran. The numbers on images represent the median dextran index calculated from >100 cells analyzed from each of two biological replicates conducted on different days; box and whisker plots represent median and quartiles. Scale bar, 20 μm. In D, F, and H, statistical significance was calculated using a one-way ANOVA with Dunn's post-hoc analysis to correct for multiple comparisons. In D, ***$p<0.001$ comparing each HeLa clonal cell line ± EIPA; \$$p<0.05$, \$\$\$$p<0.001$ comparing each clonal cell line to control HeLa cells without EIPA. In F and H, **$p<0.01$, ***$p<0.001$, ns (not significant, $p>0.05$) comparing the clonal cell lines ± EGF or Wnt3a; \$\$\$$p<0.001$ for the indicated comparisons.

1.25 μg/ml mitomycin C limited proliferation without killing HeLa cells (Figure 7E). HeLa CARMIL1-AA cell migration in a scratch assay was delayed (Figure 7, F and G). This may reflect a cell type dependent effect or an interaction between CARMIL1-AA and the poorly tolerated mitomycin C. To determine whether the slower migration in CARMIL1-AA cells reflected defective RAC activation, activated RAC GTP was measured in EGF-stimulated HeLa cells. EIPA, but not CARMIL1-AA expression, compromised RAC activation as expected (Figure 7H; Koivusalo *et al.*, 2010). Together, these results indicate that CARMIL1-AA overexpression blocks macropinocytosis without affecting cellular proliferation or RAC activation while its ability to support migration may be cell type dependent.

CARMIL1-AA does not inhibit autophagy

CARMIL1-AA limits proliferation and survival when cells are depending on macropinocytosis to supply scavenged exogenous nutrients (Jayashankar and Edinger, 2020) (Figure 5, E–G). Because CARMIL1-AA interferes with macropinocytosis through its effects on actin dynamics (Hernandez-Valladares *et al.*, 2010; Edwards *et al.*, 2013) and actin remodeling is also required for autophagosome formation, maturation, and degradation (Kast and Dominguez, 2017; Dong and Quan, 2024), it was important to evaluate whether CARMIL1-AA expression interferes with autophagy. Like macropinocytosis, autophagy supports cell survival under nutrient stress (Florey and Overholtzer, 2019; Chavez-Dominguez *et al.*, 2020; Debnath *et al.*, 2023). Moreover, autophagy plays an

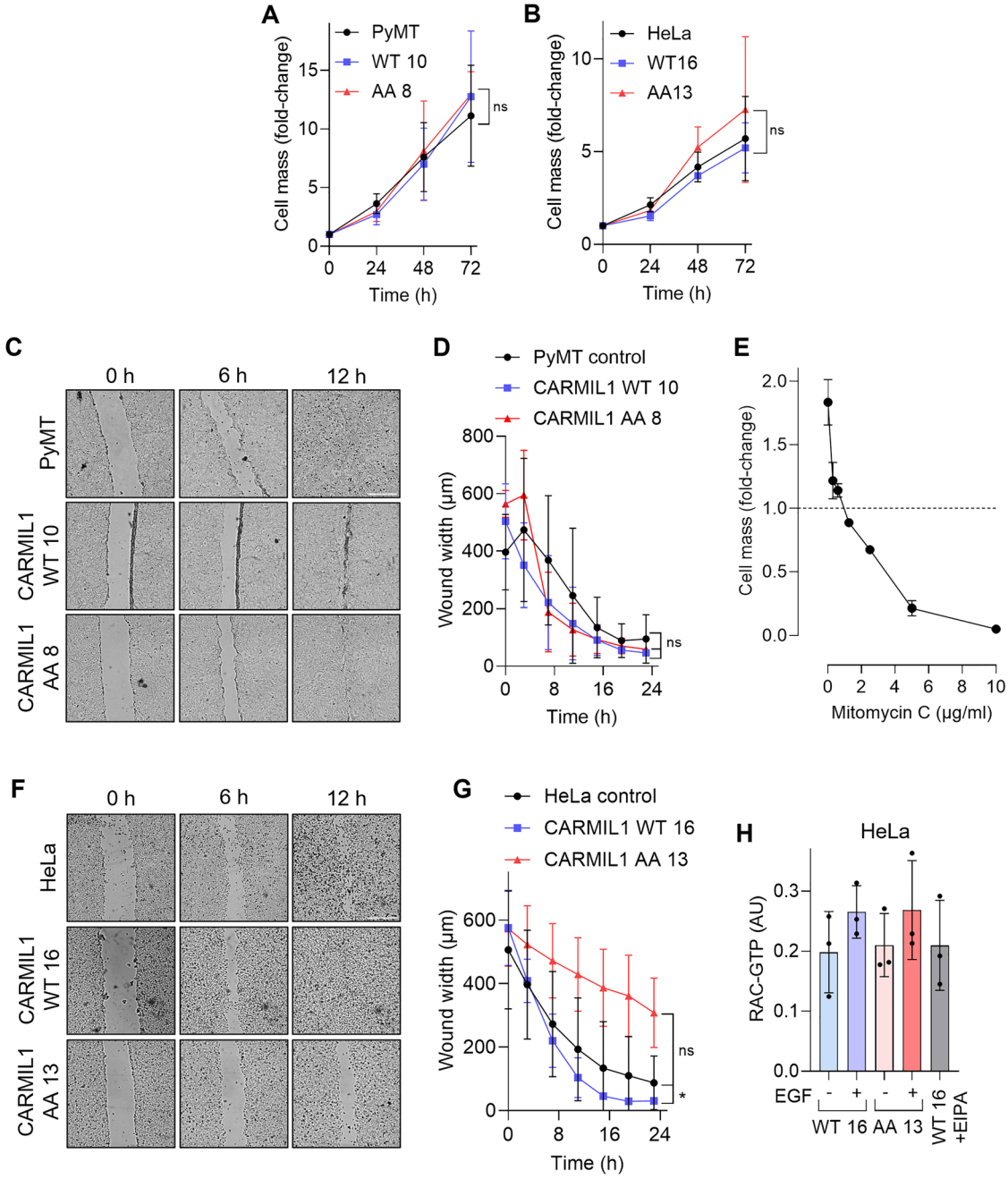

FIGURE 7: CARMIL1-AA does not inhibit proliferation, migration, or RAC activation. (A, B) Cellular proliferation was measured in complete medium by crystal violet staining for PyMT (A) and HeLa (B) control cells or clonal cell lines with matched expression of CARMIL1-WT or CARMIL1-AA. Means and SD of 3 independent biological replicates shown. (C, D) Scratch assay in control, CARMIL1-WT 10, or CARMIL1-AA 8 expressing PyMT cells pretreated with 10 µg/ml mitomycin C for 1 h in complete medium. Means and SD of three independent biological replicates shown. Scale bar, 250 µm. (E) Mitomycin C cytotoxicity in HeLa cells measured at 72 h in complete medium by crystal violet staining. Means and SD from three independent experiments shown. (F, G) Scratch assay in control and CARMIL1-WT 16 and CARMIL1-AA 13 expressing HeLa cells pretreated with 1.25 µg/ml mitomycin C for 1 h in complete media. Means and SD of three independent biological replicates shown. Scale bar, 250 µm. (H) RAC-GTP levels in HeLa control, CARMIL1-WT 16, or CARMIL1-AA 13 expressing cells measured using a RAC-GTP ELISA (G-LISA) assay. HeLa cells were serum starved overnight before pretreatment with 75 µM EIPA for 1.5 h and stimulation with 100 ng/ml EGF for 30 min. Means and SD of three biological replicates shown. In A, B, D, and G, statistical significance was calculated using a one-way ANOVA with Tukey's post-hoc analysis to correct for multiple comparisons at all timepoints measured. In A, B, D, ns, not significant, $p>0.05$ comparing all PyMT and HeLa cell lines to each other at all timepoints. In G, *$p<0.05$ comparing the HeLa CARMIL1-WT 16 to the CARMIL1-WT 13 cells at endpoint; ns = not significant, $p>0.05$ for all comparisons.

important role in shaping the antitumor immune response (de Souza *et al.*, 2020; Yamamoto *et al.*, 2020). While blocking macropinocytosis and autophagy simultaneously may be a highly effective therapeutic strategy, accurately determining the contribution macropinocytosis to tumor biology requires selective inhibition of macropinocytosis but not autophagy.

To evaluate whether CARMIL1-AA interferes with autophagy, autophagic flux was determined. LC3-II is present on both the inner and outer membranes of mature autophagosomes. While ATG4 recycles the LC3-II on the outer membrane, LC3-II on the inner autophagosomal membrane is inaccessible and thus lysosomal degradation of LC3-II is proportional to the degradation of autophagosome cargo (Kabeya *et al.*, 2004; Lee and Lee, 2016). Comparing LC3-II levels in the presence and absence of the V-ATPase inhibitor bafilomycin A1 (BafA1) permits the measurement of autophagosome degradation in the lysosome or "autophagic flux" (Mizushima and Yoshimori, 2007; Tanida *et al.*, 2008). Cancer cells are constitutively under oxidative and proteotoxic stress and often exhibit autophagic flux even in complete medium. Both PyMT and HeLa cells exhibited autophagic flux in complete medium that was increased by transfer to Hank's buffered salt solution (HBSS, nutrient stress) (Figure 8, A–C). Transferring cells to HBSS reduced LC3-II levels due to increased autophagosome degradation while BafA1 increased the levels of LC3-II in complete medium and under nutrient stress. These results demonstrate that the autophagy pathway is functional in both cell types. Autophagic flux was next examined in clonal cell lines expressing CARMIL1-WT or -AA. Both basal and nutrient stress-induced autophagic flux were similar in CARMIL1-WT and -AA PyMT and HeLa clones (Figure 8, D–G). Basal LC3-II levels were similar and BafA1 increased LC3-II levels equally in the matched PyMT and HeLa CARMIL1-WT and -AA clones. Thus, this Western blot–based autophagic flux assay following endogenous LC3-II levels suggests that CARMIL1-AA supports autophagy (Figure 8, D–G) but not macropinocytosis (Figures 4–6; Supplemental Figure S2).

A fluorescent autophagic flux probe with live-cell imaging was also utilized to measure autophagic flux over time (Figure 8H; Kaizuka *et al.*, 2016). Upon cleavage by ATG4, this probe produces equal amounts of GFP-LC3 and the control protein RFP-LC3ΔG, a mutant that cannot be conjugated to phosphatidylethanolamine, does not accumulate on autophagosomes, and that is not degraded by autophagy. A reduction in the ratio of GFP:RFP fluorescence therefore indicates that LC3-II was lost due to autophagy as RFP fluorescence serves as an internal control for reduced reporter expression or degradation through autophagy-independent pathways. Following normalization to RFP-LC3ΔG, the ratio of GFP-LC3 in the presence and absence of the lysosomal degradation inhibitor BafA1 can be used to track autophagic flux. To ensure equivalent autophagy reporter expression, a PyMT GFP-LC3-RFP-LC3ΔG clonal cell line was generated first and CARMIL1-WT or CARMIL1-AA subsequently introduced. CARMIL1-WT and -AA clones with similar CARMIL1 overexpression were identified and dextran uptake analysis used to confirm that macropinocytosis was reduced as expected after CARMIL1-AA, but not -WT, expression (Supplemental Figure S3, A–D). Autophagic flux was similar in CARMIL1-WT and -AA clones in both complete medium and HBSS (Figure 8, I and J). In sum, CARMIL1-AA did not compromise autophagy.

The effect of EIPA on autophagy was also determined. The LC3-II band in PyMT and HeLa cells maintained in complete medium intensified upon treatment with EIPA, similar to what was observed with BafA1 (Figure 8, K and L). This could mean that EIPA limits autophagosome degradation similarly to BafA1. To test this possibility, cells were incubated with both EIPA and BafA1. Blocking lysosomal degradation with BafA1 *decreased* LC3-II accumulation in EIPA-treated cells (Figure 8, K–M). A reduction in LC3-II levels upon the addition of BafA1 is not consistent with EIPA inhibiting lysosomal degradation and instead suggests that EIPA induces the conjugation of ATG8 to single membranes (CASM) (Gao *et al.*, 2016; Liu *et al.*, 2019; Durgan *et al.*, 2021; Reid *et al.*, 2022). Indeed, CASM is triggered by multiple agents that alter the pH and solute composition of endosomes and lysosomes similar to EIPA (Florey *et al.*, 2015; Jacquin *et al.*, 2017; Fletcher *et al.*, 2018; Lystad and Simonsen, 2019; Lystad *et al.*, 2019; Wang *et al.*, 2022). By triggering CASM, EIPA could reduce canonical autophagy if CASM and autophagy compete for the same pool of LC3-II. Regardless of whether or not EIPA compromises autophagic flux, the possibility that it triggers CASM raises further concerns with the practice of using EIPA to measure the contribution of macropinocytosis to tumor growth and metabolism.

In conclusion, these findings highlight the limitations of using EIPA or NHE1 knockdown to block macropinocytosis while offering an alternative approach: using the CARMIL1-AA mutant as a dominant-negative to inhibit macropinocytosis without impacting cellular proliferation or autophagy.

DISCUSSION

EIPA is the most widely used chemical inhibitor of macropinocytosis. EIPA is useful to determine the background in short-term dextran uptake assays because EIPA is selective for macropinocytosis over other endocytic processes (West *et al.*, 1989; Gekle *et al.*, 2001; Kim *et al.*, 2018). However, EIPA cannot be used to accurately measure the contribution of macropinocytosis to cell growth, proliferation, or survival *in vitro* or *in vivo*. By inhibiting NHE-dependent proton transport, EIPA will alter cellular and organellar pH leading to wide-ranging effects on cells (Steffan *et al.*, 2009; Koivusalo *et al.*, 2010; Rolver *et al.*, 2020). Intracellular pH regulates cellular metabolism, signal transduction, and protein conformation, processes that will significantly impact tumor growth independent of macropinocytosis (Orij *et al.*, 2011; Isom *et al.*, 2013; Jin *et al.*, 2022; Okreglak *et al.*, 2023). Simply by inhibiting RAC activation (Koivusalo *et al.*, 2010; Figure 7H), EIPA will have profound macropinocytosis-independent effects on cell cycle progression, transformation, and migration (Stock *et al.*, 2005; Spear and White, 2023; Romero-Moreno *et al.*, 2024). In contrast, blocking macropinocytosis with CARMIL1-AA expression did not hinder cellular proliferation under conditions where cell proliferation and survival is dramatically reduced by EIPA (Figures 7, A and B and 1, F and G). These data strongly support the conclusion that EIPA's effects on proliferation are macropinocytosis-independent. For example, HeLa clone AA 13 has the same dextran index as cells treated with 75 μM EIPA (Figure 6, C and D); this same clone has no proliferation defect (Figure 7B) unlike cells treated with 75 μM EIPA (Figure 1G). Clone PyMT AA 8 also proliferates normally (Figure 7A) but has a slightly higher dextran index than cells treated with 75 μM EIPA (dextran indices of 4.4 vs. 3.0, respectively in Figure 4, G and H). However, PyMT cells treated with 20 μM EIPA have dextran index of 7.5 (Figure 1, C and D) and reduced proliferation (Figure 1F). It therefore is very likely that EIPA suppresses proliferation through macropinocytosis-independent mechanisms. EIPA may also negatively affect autophagy, a process that is important for tumor growth, as expected for a compound that affects cellular and endosomal pH and ion content (Durgan and Florey, 2022; Wang *et al.*, 2022), EIPA appears to induce CASM (Figure 8, K–M).

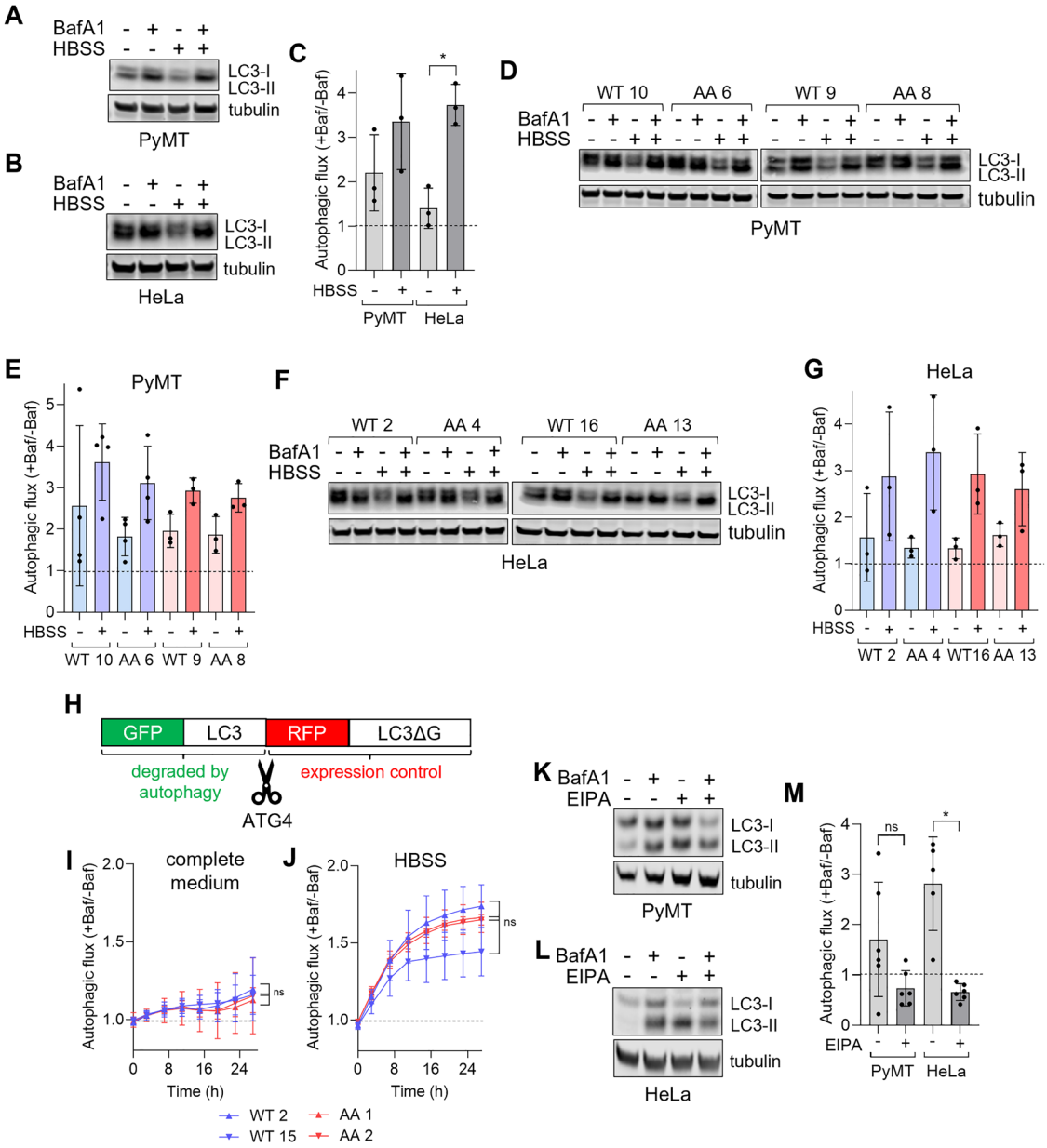

FIGURE 8: CARMIL1-AA supports autophagy. A and B, Western blot in PyMT (A) or HeLa (B) cells treated with 250 nM BafA1 in complete medium or HBSS for 2 h. LC3-II is the lower band. (C) Autophagic flux calculated from three independent biological replicates, mean ± SD shown. (D–G) Western blots in PyMT (D) or HeLa (F) CARMIL1-WT and CARMIL1-AA expressing clonal cell lines maintained for 2 h ± 250 nM BafA1 in complete medium or HBSS. (E, G) Autophagic flux in PyMT (D) or HeLa (F) cells calculated from three independent biological replicates, mean ± SD shown. (H) Schematic for the GFP-LC3-RFP-LC3ΔG probe. (I, J) Autophagic flux analysis in PyMT GFP-LC3-RFP-LC3ΔG clones expressing CARMIL1-WT or CARMIL1-AA either in complete media (I) or in HBSS (J). Autophagic flux was calculated by taking the ratio of GFP:RFP+BafA1/GFP:RFP-BafA1 (100 nM BafA1). (K-M) As in (A-C) but PyMT (K) or HeLa (L) cells were treated with 75 μM EIPA in complete medium for 1.5 h. (M) Mean ± SD for 5–6 independent experiments shown. In C, E, G, I, J, and M, statistical significance was calculated using a one-way ANOVA with Tukey's post-hoc analysis to correct for multiple comparisons. In C, *$p<0.05$ comparing HeLa cells ± HBSS. In I and J, ns = not significant, $p>0.05$ comparing matched CARMIL1-WT or -AA PyMT clones to each other. In M, *$p<0.05$, ns = not significant, $p>0.05$ for the indicated comparisons.

How CASM may affect cancer initiation and progression is not yet clear, but it is a reasonable assumption that inducing CASM could reduce the amount of LC3-II available for autophagy or otherwise disrupt processes important for tumorigenesis. In sum, the macropinocytosis-independent effects of EIPA should preclude its use to accurately define the contribution macropinocytosis makes to tumor cell proliferation or survival *in vitro* or *in vivo*.

Targeting only the NHE1 isoform is not a solution to the specificity problems of EIPA. By modulating cytosolic pH, NHE1 inhibition or knockdown has multiple macropinocytosis-independent effects on tumor phenotypes (Jenkins *et al.*, 2012;

Stock and Pedersen, 2017; Cheng *et al.*, 2019). More importantly, NHE1 knockdown failed to block macropinocytosis in HeLa and MDA-MB-231 cell lines where EIPA is effective (Figure 2, A–H). Published studies where NHE1 knockdown was used to block macropinocytosis did not validate this approach using standard assays in the field, 70 kD dextran uptake or live-cell imaging, calling into question whether the phenotypes observed were related to effects on pH rather than macropinocytosis and whether *NHE1* should be included as part of a macropinocytosis-related gene expression signature (Su *et al.*, 2021; Lin *et al.*, 2022). Which NHE isoform(s) is/are required for macropinocytosis remains uncertain, and targeting these proteins is unlikely to selectively inhibit macropinocytosis due to their important role in pH regulation.

Several FDA-approved drugs, such as imipramine and phenoxybenzamine, inhibit macropinocytosis without exerting cytotoxic effects (Lin *et al.*, 2018). However, the lactate dehydrogenase (LDH) release assay used in this study would be unlikely to detect proliferation decreases. The best compounds from this study, phenoxybenzamine and imipramine, inhibit membrane ruffling suggesting that other RAC-dependent processes (e.g., proliferation) may be impacted. Imipramine is also structurally very similar to phenothiazines that have been demonstrated to activate PP2A (Gutierrez *et al.*, 2014). Given that these compounds are FDA-approved based on their macropinocytosis-independent actions, they would not be useful to isolate the effects of macropinocytosis on tumor biology *in vivo*. Other compounds targeting processes essential for macropinocytosis such as actin polymerization (Cytochalasin D), PI3K activation (Wortmannin/LY294002, ZSTK474), or V-ATPase mediated acidification (Bafilomycin A1) inhibit macropinocytosis but would affect numerous other cellular process that are important for cancer cell proliferation and survival (Amyere *et al.*, 2000; Stockinger *et al.*, 2006; Araki *et al.*, 2007; Koivusalo *et al.*, 2010; Kitazawa *et al.*, 2017; Qiu *et al.*, 2022). At this time, there is no chemical inhibitor available that inhibits macropinocytosis without affecting other tumor promoting processes.

CARMIL1-AA was reported to selectively inhibit macropinocytosis in the context of endogenous CARMIL1 knockdown (Edwards *et al.*, 2013). Here we show that the overexpression of CARMIL1-AA was sufficient to reduce dextran uptake and macropinosome formation in both PyMT and HeLa cells exposed to various macropinocytosis-inducing stimuli even in the presence of endogenous CARMIL1 (Figures 4 and 6; Supplemental Videos S4 and S5). In fact, CARMIL1-AA expression reduced macropinocytosis to a greater extent than CRISPR/Cas9 mediated CARMIL1 knockdown, and CARMIL1 knockdown in CARMIL1-AA expressing cells did not improve macropinocytosis inhibition (Figures 3, 4, and 6; Supplemental Figure S1). Superior inhibition of macropinocytosis when CARMIL1-AA is expressed in the presence of endogenous CARMIL1 might be explained if knockdown induces compensatory changes in gene expression or protein stability as part of an adaptive response to the loss of CARMIL1. The possibility that clonal variation might account for the reduced macropinocytosis following CARMIL1-AA expression without knockdown was ruled out by demonstrating that acute induction of CARMIL1-AA expression with doxycycline inhibited macropinocytosis to a similar extent as constitutive CARMIL1-AA expression and EIPA (Figures 4; Supplemental Figure S2). The finding that CARMIL1-AA functions as a dominant-negative mutant is consistent with CARMIL1 function as a homodimer (Zwolak *et al.*, 2013; Wang *et al.*, 2016). It remains to be tested whether the CARMIL1-AA mutant will be an effective inhibitor of macropinocytosis across all cancer cell lines and in myeloid cells. However, it is promising that this mutant is effective in blocking macropinocytosis in response to nutrient stress, PMA, EGF, and Wnt3a and in multiple cancer cell types (Figures 4–6).

CARMIL1-AA did not inhibit RAC activation in response to EGF (Figure 7H). Consistent with the role of RAC-GTP in cell cycle progression, membrane ruffling, and migration (Miki *et al.*, 1998; Koivusalo *et al.*, 2010), PyMT cells expressing CARMIL1-WT or CARMIL1-AA proliferated (Figure 7A), ruffled (Supplemental Videos S4 and S5), and migrated (Figure 7, C and D) at similar rates. The reduced migration in CARMIL1-AA–expressing HeLa cells may result from a negative interaction with mitomycin C or may reflect a difference between cell types. It was particularly important to evaluate the effect of CARMIL1-AA on autophagy because actin plays a critical role in the formation of both macropinosomes and autophagosomes (Miki *et al.*, 1998; Veltman *et al.*, 2016; Kast and Dominguez, 2017; Mylvaganam *et al.*, 2021; Palm, 2022; Dong and Quan, 2024). Both macropinocytosis and autophagy can support cancer cell survival in nutrient-limiting environments and promote drug resistance (Zhang *et al.*, 2017; Jayashankar *et al.*, 2018; Kim *et al.*, 2018; Chavez-Dominguez *et al.*, 2020; Jayashankar and Edinger, 2020; Li *et al.*, 2020; Actis *et al.*, 2021; Debnath *et al.*, 2023). Our novel finding that CARMIL1-AA did not limit or induce autophagic flux (Figure 8) is thus particularly significant because it establishes a way to separate the contributions of macropinocytosis and autophagy. In conclusion, the CARMIL1-AA mutant provides a means to dissect the contribution macropinocytosis makes to tumor initiation, progression, and therapeutic resistance without compromising autophagy or proliferation.

MATERIALS AND METHODS

Request a protocol through *Bio-protocol*

Cell lines and cell culture

HeLa, MDA-MB-231, and HEK293T cells were obtained from the ATCC (Manassas, VA, United States) and validated via STR profiling at the initiation of the project. FL5.12 cells were originally obtained from Craig Thompson's lab (UC Irvine, CA, United States). The PyMT mammary cancer cell line was generated from a tumor in an FVB/NJ mouse from the polyomavirus middle T antigen model (MMTV-PyMT) and was a generous gift from Dr. Jennifer Prescher (UC Irvine, CA, United States). All cells were cultured at 37°C and 5% CO_2 in a humidified incubator in media supplemented with 10% FBS (Omega Scientific, Tarzana, CA, United States). Media formulations were purchased from Life Technologies through Thermo Fisher Scientific (Waltham, MA, United States). HeLa and HEK293T cells were cultured in DMEM, MDA-MB-231 cells in DMEM with 1 mM sodium pyruvate, FL5.12 cells in ATCC-Modified RPMI media supplemented with 50 μM β-mercaptoethanol, penicillin/streptomycin, and 100 ng/ml murine rIL-3, and PyMT cells in DMEM/F-12. For nutrient limitation, DMEM/F-12 media containing 1% of the normal level of amino acids and glucose (1% AA/gluc) was prepared by making DMEM/F-12 lacking amino acids and glucose from chemical components and mixing it 99:1 with purchased complete medium. Where gene expression was induced with doxycycline cells were cultured in certified tetracycline-free serum (Omega Scientific, Tarzana, CA, United States). All cells tested negative for *Mycoplasma* by PCR analysis (Uphoff and Drexler, 2014) conducted every 1–3 mo throughout the project. MDA-MB-231, HeLa, and PyMT cells were transfected using Lipofectamine 3000 (Thermo Fisher Scientific, Waltham, MA, United States). Cells were selected with 2 μg/ml puromycin (Thermo Fisher Scientific, catalogue no. AC227420100, Waltham,

MA, United States) 48 h after transfection then cloned by limiting dilution. Constitutive or doxycycline-inducible CARMIL1-WT or -AA expression in PyMT and HeLa cells was achieved by lentiviral transduction followed by drug selection with 200–800 μg/ml geneticin sulfate (VWR, catalogue no. 89149-808, Radnor, PA, United States) and cloning by limiting dilution. pMRX-IP-GFP-LC3-RFP-LC3ΔG (a gift from Noboru Mizushima, Addgene plasmid # 84572, [Kaizuka *et al.*, 2016]) was used to introduce GFP-LC3-RFP-LC3ΔG into cells by lentiviral transduction.

Antibodies and other reagents

Antibodies were obtained from: beta Tubulin (MilliporeSigma, catalogue no. T4026, Burlington, MA, United States); LC3 A/B (Cell Signaling Technology, catalogue no. 4108S, Danvers, MA, United States), LRRC16A/CARMIL1 (Thermo Fisher Scientific, catalogue no. PIPA556045, Waltham, MA, United States), NHE-1 (Santa Cruz Biotechnology, catalogue no. sc-136239, Dallas, TX, United States). The 70 kDa Oregon Green 488 Dextran was from Thermo Fisher Scientific (catalogue no. D7173, Waltham, MA, United States), the 70 kDa CF 633 Dextran was purchased from Biotium (catalogue no. 80141 Fremont, CA, United States). DAPI was obtained from BioLegend (catalogue no. 422801, San Diego, CA, United States) and Hoechst 33342 from Thermo Fisher Scientific (catalogue no. H3570, Waltham, MA, United States). All plasmids were purchased either from Addgene (Watertown, MA, United States) or from Thermo Fisher Scientific (Waltham, MA, United States).

Molecular cloning

The CARMIL1 wild type and AA point mutant cDNA were initially obtained from John Cooper (Washington University) in the pFLRu vector. The pSIN4-EF2-ABCG2-IRES-Neo (a gift from Ren-he Xu, Addgene plasmid # 25983 [Zeng *et al.*, 2009]) was utilized to constitutively overexpress CARMIL1-WT or -AA. The CARMIL1 ORF was cloned from the pFLRu vector into the pSIN4 vector using EcoRI and BamHI sites. pInducer20 (a gift from Stephen Elledge, Addgene plasmid # 44012 [Meerbrey *et al.*, 2011]) was utilized for doxycycline-inducible expression of CARMIL1-WT or -AA using Gateway cloning from pDONR221 (Thermo Fisher Scientific, Catalogue No. 12536017) with a CARMIL1-WT or -AA insert created by PCR. For CRISPR-mediated knockdown of endogenous NHE1 and CARMIL1, pLentiCRISPR v2 (a gift from Feng Zhang, Addgene plasmid # 52961 [Sanjana *et al.*, 2014]) was used to transiently transfect (not transduce) target cells which were then drug selected and cloned by limiting dilution after 48 h. The sgRNAs targeting NHE1 and endogenous mouse and human CARMIL1 were cloned as recommended in the Zheng lab's protocol on Addgene. sgRNA sequences were:

NHE1 Guide 1 (Exon 2) Forward: 5′ CACCATCCTGATCTTTGCCG 3′
NHE1 Guide 1 (Exon 2) Reverse: 5′ CGGCAAAGATCAGGATGGTG 3′
NHE1 Guide 2 (Exon 1) Forward: 5′ CCAATCGAGCGTTCTCGTGG 3′
NHE1 Guide 2 (Exon 1) Reverse: 5′ CCACGAGAACGCTCGATTGG 3′
Mouse CARMIL1 Guide 1 Forward: 5′ CACCGTAACTCGAGCTGTAATGAGGGGG 3′
Mouse CARMIL1 Guide 1 Reverse: 5′ AAACCCCCCTCATTACAGCTCGAGTTAC 3′
Human CARMIL1 Guide 1 Forward: 5′ CACCGCCGGTTCTTGCAGATGATTG 3′
Human CARMIL1 Guide 1 Reverse: 5′ AAACCAATCATCTGCAAGAACCGGC 3′

All the CARMIL1 sgRNAs target intron-exon junctions (between Exons 3 and 4 for the mouse guides and between Exons 4 and 5 for the human guides) to avoid Cas9 targeting and cleavage of the exogenous CARMIL1 cDNAs.

Western blot analysis

Cells were lysed in RIPA buffer (1% sodium deoxycholate, 0.1% sodium dodecyl sulfate, 1% Triton-X100, 25 mM Tris pH 8.0, 150 mM sodium chloride, and 0.25% sodium azide) supplemented with cOmplete protease inhibitor cocktail (Roche, Indianapolis, IN, United States). Protein concentration was determined by bicinchoninic acid (BCA) Assay (Thermo Fisher Scientific, Waltham, MA, United States). Equal amounts of protein (20 μg) were run per lane on a NuPAGE Novex 4–12% Bis-Tris gel (Invitrogen, Calsbad, CA, United States), transferred to a nitrocellulose membrane either by wet transfer for 2–3 h at 30 V (Bis-Tris transfer buffer recipe: 25 mM Bicine, 25 mM Bis-Tris free base, and 1 mM EDTA at pH 7.2) or by semidry transfer using the iBlot3 (Invitrogen, Calsbad, CA, United States) at 25 V for 10 min with no cooling. Membranes were blocked with 5% BSA solution for 1 h before incubation with primary antibodies (1:1000 dilution for anti-NHE1, anti-CARMIL1, and anti-LC3 A/B and 1:20,000 dilution for anti-beta tubulin) diluted in 5% BSA blocking buffer at 4°C overnight. Membranes were washed 3 × 5 min with 1X Tris-Buffered Saline solution with 0.05% Tween20 (TBS-T) before addition of IRDye 680 or 800 conjugated secondary antibodies at a 1:10,000 dilution in 5% BSA block solution (LI-COR Biotechnology, Lincoln, Nebraska, United States) for 1 h at room temperature. Membranes were washed with TBS-T and imaged on a LI-COR Odyssey Clx Scanner (LI-COR Biotechnology, Lincoln, Nebraska, United States).

Microscopy

Cells were plated at 20,000 per well in an 8-well glass chamber slide (CellVis, catalogue no. C8-1.5H-N). The following day, macropinocytosis was induced. PyMT cells were washed 3X with PBS before incubation in 1% AA/glucose DMEM-F12 media for 6 h unless otherwise noted. HeLa cells were stimulated with 250 nM PMA (Cayman Chemicals, catalogue no. 10008014, diluted in DMSO) for 30 min. MDA-MB-231 cells are constitutively macropinocytic (Jayashankar and Edinger, 2020). In each experiment, one sample was treated with 10, 20, 50, or 75 μM EIPA for 90 min total (1 h preincubation, last 30 min with addition of dextran) to block macropinocytosis. To label macropinosomes, cells were incubated in 1 mg/ml 70 kD Oregon Green Dextran (Thermo Fisher Scientific, diluted in 1X PBS) or 0.5 mg/ml CF 633 Dextran (Biotium, diluted in 1X PBS) for 30 min at 37°C. Samples were washed 5X in PBS before fixation with 4% paraformaldehyde for 15 min at room temperature. The cells were washed one more time with PBS before nuclei were stained with either 5 μg/ml DAPI or Hoechst 33342 (both diluted in 1X PBS) for 5 min at room temperature before imaging. Where doxycycline induction was required, PyMT CARMIL1-WT and -AA cells were plated at 12,000 cells/well and treated the next day with 1 μg/ml doxycycline in complete media for 48 h before nutrient stress as above. For experiments involving EGF (Thermo Fisher Scientific, catalogue no. PHG0311, Waltham, MA, United States), HeLa CARMIL1-WT and -AA cells were washed 3X with PBS before overnight serum starvation. Cells were stimulated with 100 ng/ml EGF for 30 min at the time of dextran addition. For Wnt3a (Peprotech, catalogue no. 315-20, Cranbury, NJ, United States) stimulation, cells were serum starved for 6

h in the presence of 20 μg/ml cycloheximide (VWR, catalogue no. 97064-724, Radnor, PA, United States) for the last 4 h of incubation to limit Wnt3a secretion before the addition of 100 ng/ml Wnt3a simultaneously with dextran.

CFSE-labeled necrotic debris was generated from FL5.12 cells. Approximately 100 million cells were washed 3X with PBS then incubated with 1.25 μM CFSE (Thermo Fisher Scientific, catalogue no. C34570, dissolved in DMSO) in PBS containing 2% FBS for 5 min at room temperature. Cells were then washed 3X with PBS then resuspended at ∼200 million cells/ml in PBS. Debris was harvested after 10 d of incubation at 37°C and 5% CO_2 in a humidified incubator. The supernatant from a 3-min spin at 400 × *g* was collected and confirmed by widefield imaging to contain primarily necrotic debris and few apoptotic cells. Apoptotic cells were generated by IL-3 withdrawal from FL5.12 cells. A total of 10 million FL5.12 cells were washed 3X with PBS, stained with CFSE, washed 3X with PBS, and resuspended in FL5.12 media lacking IL-3 at a density of 1 million cells/ml for 24 h. Where uptake of CFSE-labeled debris or apoptotic cells was performed, PyMT cells were plated in 8-well chamber slides and incubated with 2 million cell equivalents of necrotic debris per well for the last 2 h of the 6 h of nutrient deprivation. Samples were then processed as for dextran imaging.

Dextran and necrotic debris uptake were analyzed on a Zeiss LSM 900 with Airyscan 2 laser-scanning confocal microscope (Zeiss, Oberkochen, Germany) equipped with the Axiocam 503 mono camera using the Plan-Apochromat 63X/1.40 oil DIC objective for all dextran and CFSE-FL5.12-labeled necrotic uptake assays. The Zeiss ZEN 3.0 Software was used for image acquisition. The maximum gain and laser power for the nuclei and dextran channels were determined based on the range indicator, in which the nuclei turned up partially red and gray and the majority of the labeled macropinosomes were colored red. Saturation of the dextran channel was permitted for this experiment because the measured parameter is the %area of the cell that contained dextran rather than fluorescence intensity. Z-stacks were collected with a step size of 0.5 μm and 10–20 stacks were obtained from a total of 3–5 fields of view (FOV) per sample containing at least 100 cells per biological replicate. FOV were primarily determined based on the DAPI/Hoechst channel, trying to take in about 20–30 cells per FOV while avoiding apoptotic/necrotic cells. Microscope acquisition settings were held constant between different conditions in the same experiment and adjusted for each experiment using positive and negative controls including highly-macropinocytic cells (MDA-MB-231 cells or nutrient-stressed PyMT cells) as the positive control and EIPA-treated cells as the negative control. CFSE-labeled FL5.12 necrotic debris was imaged using the Plan Fluor 100X/1.30 Oil DIC H/N2 objective (Nikon, Melville, NY, United States) and a Nikon Eclipse Ti2-A microscope (Nikon, Melville, NY, United States) equipped with the SOLA U-NIR White LED Light Engine Gen III 350–760 nm and the PCO Panda USB3.0 sCMOS camera. Images were acquired using the NIS-Elements Basic Research software (Nikon, Melville, NY, United States) and processed on Fiji (Image J, NIH, Bethesda, MD, United States).

Live-cell imaging

For holotomographic imaging on a Nanolive 3D Cell Explorer (Nanolive, Tolochenaz, Switzerland), 75,000 PyMT cells were plated in 35 mm imaging dishes (Ibidi, catalogue no. 80136). To induce macropinocytosis, cells were washed 3X with PBS then imaged after a 6-h incubation in 1% AA/glucose DMEM-F12 media. Three to five FOV were imaged for each sample and images were collected every 10 s for 2 h. The number of macropinosomes per cell was determined manually.

Dextran analysis

Dextran uptake was determined on a per cell basis using Fiji (Image J, NIH, Bethesda, MD, United States). Cells were manually outlined on the merged DAPI and brightfield channels using the free-hand tool. Cells in mitosis, undergoing apoptosis (fragmented nuclei in the DAPI channel) or that were not entirely within the FOV were excluded from the analysis. A maximum intensity projection (MIP) was generated for the full dextran z-stack and thresholded equally among all experiment groups and FOV using the Brightness and Contrast setting to adjust the image so that there was no signal outside of the cell boundaries using the image containing the most noise outside the cell (usually EIPA-treated cells). The MIP was converted to a binary image and the analyze particles tool was used to calculate the percent of the cellular area positive for dextran (dextran index) for each region of interest (ROI). The dextran index shown in representative MPI images is the median percent area from ∼ 100 cells from each of at least two biological replicates conducted on different days.

Necrotic cell rescue assays

For the necrotic uptake rescue experiments, necrotic debris was generated from FL5.12 cells by inducing growth factor and nutrient deprivation simultaneously. Approximately 100 million cells from a culture maintained at a density of ∼1 million cells/ml were washed 3X with PBS and resuspended at a density of 200 million cells/ml in PBS and incubated for 10 d at 37°C in a humidified incubator with 5% CO_2. To collect the necrotic debris, the cells were subjected to a quick spin (400 × *g* for 3 min) using the accuSpin microcentrifuge (Thermo Fisher Scientific, Waltham, MA, United States), and the supernatant was collected. The necrotic debris was then pelleted (2,800 × *g* for 10 min) and resuspended in DMEM containing 1 μM doxorubicin (Cayman Chemicals, catalogue no. 15007, Ann Arbor, MI, United States, dissolved in DMSO) for addition to cells. A total of 10 million necrotic cell equivalents were added to PyMT cells treated with 1 μM doxorubicin in a 24-well plate. At 96 h, PyMT cells were imaged (widefield) then stained with crystal violet (0.5% crystal violet [catalogue no. C581100 from Thermo Fisher Scientific] in 20% methanol). Crystal violet was quantified by drying the plates, solubilizing crystal violet with 100% methanol for 15 min at room temperature and determining the absorbance at 595 nm on a Bio-Tek EL800 plate reader (Bio-Tek, Shoreline, WA, United States) using the Gen5 software (Agilent Technologies, Inc., Santa Clara, CA, United States).

Autophagy assays

For Western blot autophagic flux assays, PyMT or HeLa cells were plated at 300,000 cells/well in a 6-well plate. The following day, cells were washed 3X with PBS and incubated in HBSS containing calcium and magnesium (catalogue no. 14025076, Thermo Fisher Scientific, Waltham, MA, United States) or complete medium ± 250 nM Bafilomycin A1 (BafA1, Cayman Chemicals, Ann Arbor, MI, United States, dissolved in DMSO) as indicated for 2 h at 37°C before lysis and analysis by Western blot. Autophagic flux was determined by normalizing the LC3-II signal to tubulin and then expressing a ratio of +BafA1/−BafA1. Where indicated, cells were incubated with 75 μM EIPA in complete media for 4 h at 37°C before lysis and analysis of LC3-II by Western blotting. For the fluorescence-based flux analysis, PyMT CARMIL1-WT or -AA GFP-LC3-RFP-LC3ΔG cells were plated at ∼12,000 cells/well in a

96-well plate and washed and treated the next day with complete medium or HBSS ± 100 nM BafA1. Cells were imaged on the Biotek Biospa Live Cell Analysis platform (Agilent, Santa Clara, CA, United States) to perform widefield microscopy every 4 h while maintaining cells at 37°C and 5% CO_2. Image capture settings were set to 4x magnification, three image filters were used: brightfield high contrast, Texas Red, and GFP. Capture settings were set to autoexposure and laser autofocus. The resulting images were then analyzed using the associated Gen5 software (version 3.12). Cell count and object sum area were calculated for each of the three image filters (brightfield, Texas Red, GFP). For brightfield high contrast, analysis settings were adjusted as follows: a threshold value of 5000 to 7000, a rolling ball diameter of 30 to 50 µm, a minimum object size 10 µm, and a maximum object size 100 µm. All other analysis settings were kept at default/auto detect settings for brightfield images. For GFP and Texas Red images, analysis settings were adjusted as follows: a threshold value of 3000–7000, a minimum object size of 5 µm, and a maximum object size of 500 µm. Rolling ball diameter and other settings were kept at default/auto detect settings for GFP and Texas Red images. The ratio of the GFP to the RFP sum areas with or without BafA1 addition was calculated to assess levels of autophagic flux over time.

Proliferation and scratch assays

PyMT or HeLa cells were plated in triplicate at 15,000 cells/well in a 24-well plate. The following day, cells were treated with vehicle, 10, 20, 50, or 75 µM EIPA in complete media then imaged on the Cytation every 4 h to measure proliferation. Images were captured using the automated Biotek Biospa Live Cell Analysis platform (Agilent, Santa Clara, CA, United States) with the same settings as for the fluorescent autophagic flux probe assay (37°C, 5% CO_2, 4X magnification with the brightfield high-contrast filter) for 4 h every 72 h. Cell count, object sum area, image width, and image height were calculated on the Gen5 software (version 3.12). Analysis settings were adjusted as follows: a threshold value of 5000 to 7000, a rolling ball diameter of 30 to 50 µm, a minimum object size 10 µm, and a maximum object size 100 µm. All other analysis settings were kept at default/auto detect settings for brightfield images. Percent confluency was calculated using the following formula: ((object sum area/(total image width x total image height)) x 100). The final %confluence of the cells was graphed to assess for overall cell growth over time.

For the HeLa and PyMT CARMIL1-WT/-AA crystal violet proliferation assays, cells were seeded in 24-well plates (20,000 cells/well) and incubated for 24, 48, 72, or 96 h. Wells without cells were prepared for the blank. After incubation, plates were washed once with 1X PBS and stained with crystal violet stain solution for 1 h. The plates were washed four times with 1X PBS then dried for 24 h. Crystal violet was solubilized with 100% methanol and the absorbance at 594 nm measured. After background subtraction, the proliferation rate was calculated as a fold change of the corrected absorbance at 48, 72, and 96 h compared with the 24 h timepoint.

For scratch assays, PyMT or HeLa cells were plated at 100,000 or 150,000 cells/well respectively in a 24-well plate and allowed to reach 100% confluence before treatment with 10 or 1.25 µg/ml Mitomycin C for 1 h before two vertical scratches were manually generated in each well using a 200 µl pipette tip. Cell migration was monitored using the same settings on the Biospa platform (37°C, 5% CO_2, 4X magnification using the brightfield high-contrast filter) for 4 h every 96 h. Beacons were set in the imaging software prior to image acquisition, indicating where the scratches were located in the well. The resulting images were then analyzed using the associated Gen5 software (version 3.12). Cell object size, object area, object sum area, image width, and image height were calculated. Analysis settings were adjusted as follows: a threshold value of 1900, background "dark," split touching objects "no," include edge objects "yes," a rolling ball diameter of 40 µm, an image smoothing strength of 20, background evaluation on 1% of lowest pixels, a minimum object size 100 µm, and a maximum object size 10,000 µm. All other analysis settings were kept at default/auto detect settings for brightfield images. Wound width was calculated using the following formula (((total image height x total image width) − Object sum area)/total image height). These settings and formula match what the Gen5 software recommends for scratch assays in the Help Topics folder within the software.

RAC activation assay

RAC activation in HeLa CARMIL1-WT and -AA cells was assessed using the Rac 1, 2, 3 G-LISA Activation Assay (catalogue no. BK125, Cytoskeleton, Inc., Denver, CO, United States) following the manufacturer's instructions. Briefly, cells were plated at ~200,000 cells/well in a 6-well plate. The following day, cells were washed 3X with PBS then incubated in DMEM without FBS for 18 h before pretreatment with or without 75 µM EIPA ± 100 ng/ml EGF for 30 min. Lysates were collected, assessed for protein concentration using the Precision Red Advanced protein assay reagent provided with the kit, and flash-frozen in liquid nitrogen. 1 mg/ml lysate was loaded in duplicate wells of the Rac G-LISA assay with absorbance at 490 nm measured on a Bio-Tek Synergy HTX multimode plate reader (Bio-Tek, Shoreline, WA, United States).

Statistical analysis

Statistical analysis was conducted using GraphPad Prism version 10 (Boston, MA, United States). In box plots, boxes depict the median dextran index with the 25th and 75th quartiles while the whiskers represent minimum and maximum values. Data comparisons were performed using a one-way ANOVA followed by Dunnett's or Tukey's test to correct for multiple comparisons. Unless otherwise indicated, bar graphs depict mean ± SD and *, $p \leq 0.05$; **, $p \leq 0.01$; ***, $p \leq 0.001$; and ns, not significant ($p > 0.05$). In dextran assays, ~100 cells were evaluated in at least two independent experiments conducted on different days. In other experiments, at least three independent biological replicates were performed.

Data availability

All relevant data can be found within the article and its Supplementary Information.

ACKNOWLEDGMENTS

The authors would like to thank Dr. Katie Sanders for generating the NHE1 knockout HeLa cells and Kazumi Eckenstein for generating the pDONR221 CARMIL1-WT and CARMIL1-AA entry vectors that were utilized for cloning into the pInducer20 destination vector. The authors would additionally like to thank Dr. Adeela Syed from the UCI Optical Biology Core Facility for providing insight into acquiring the data for the dextran and CFSE-necrotic uptake experiments.

Funding

This work was supported by grants from the National Institutes of Health (R01CA247556 to A.L.E., R37CA283575 to C.J.H.), a Tower Cancer Research Foundation Career Development Award in Translational Cancer Research (C.J.H.), an Anti-Cancer Challenge Pilot Grant Program (A.L.E., C.J.H.), and by support for R.M.L. from

5T32CA009054-42 and the American Cancer Society (PF-22-133-01-IBCD to R.M.L.).

REFERENCES

Actis C, Muzio G, Autelli R (2021). Autophagy triggers tamoxifen resistance in human breast cancer cells by preventing drug-induced lysosomal damage. Cancers (Basel) 13, 1252.

Amyere M, Payrastre B, Krause U, Van Der Smissen P, Veithen A, Courtoy PJ (2000). Constitutive macropinocytosis in oncogene-transformed fibroblasts depends on sequential permanent activation of phosphoinositide 3-kinase and phospholipase C. Mol Biol Cell 11, 3453–3467.

Araki N, Egami Y, Watanabe Y, Hatae T (2007). Phosphoinositide metabolism during membrane ruffling and macropinosome formation in EGF-stimulated A431 cells. Exp Cell Res 313, 1496–1507.

Araki N, Johnson MT, Swanson JA (1996). A role for phosphoinositide 3-kinase in the completion of macropinocytosis and phagocytosis by macrophages. J Cell Biol 135, 1249–1260.

Bar-Sagi D, Feramisco JR (1986). Induction of membrane ruffling and fluid-phase pinocytosis in quiescent fibroblasts by ras proteins. Science 233, 1061–1068.

Brown KK, Spinelli JB, Asara JM, Toker A (2017). Adaptive reprogramming of de novo pyrimidine synthesis is a metabolic vulnerability in triple-negative breast cancer. Cancer Discov 7, 391–399.

Chavez-Dominguez R, Perez-Medina M, Lopez-Gonzalez JS, Galicia-Velasco M, Aguilar-Cazares D (2020). The double-edge sword of autophagy in cancer: From tumor suppression to pro-tumor activity. Front Oncol 10, 578418.

Cheng P-C, Lin H-Y, Chen Y-S, Cheng R-C, Su H-C, Huang R-C (2019). The Na+/H+-exchanger NHE1 regulates extra- and intracellular pH and Nimodipine-sensitive [Ca2+]i in the Suprachiasmatic nucleus. Sci Rep 9, 6430.

Commisso C, Davidson SM, Soydaner-Azeloglu RG, Parker SJ, Kamphorst JJ, Hackett S, *et al.* (2013). Macropinocytosis of protein is an amino acid supply route in Ras-transformed cells. Nature 497, 633–637.

Debnath J, Gammoh N, Ryan KM (2023). Autophagy and autophagy-related pathways in cancer. Nat Rev Mol Cell Biol 24, 560–575.

de Souza ASC, Gonçalves LB, Lepique AP, de Araujo-Souza PS (2020). The role of autophagy in tumor immunology-complex mechanisms that may be explored therapeutically. Front Oncol 10, 603661.

Dong Y, Quan C (2024). NPFs-mediated actin cytoskeleton: a new viewpoint on autophagy regulation. Cell Commun Signal 22, 111.

Durgan J, Florey O (2022). Many roads lead to CASM: Diverse stimuli of noncanonical autophagy share a unifying molecular mechanism. Sci Adv 8, eabo1274.

Durgan J, Lystad AH, Sloan K, Carlsson SR, Wilson MI, Marcassa E, *et al.* (2021). Non-canonical autophagy drives alternative ATG8 conjugation to phosphatidylserine. Mol Cell 81, 2031–2040.e8.

Edinger AL, Thompson CB (2002). Akt maintains cell size and survival by increasing mTOR-dependent nutrient uptake. Mol Biol Cell 13, 2276–2288.

Edwards M, Liang Y, Kim T, Cooper JA (2013). Physiological role of the interaction between CARMIL1 and capping protein. Mol Biol Cell 24, 3047–3055.

Finicle BT, Jayashankar V, Edinger AL (2018) Nutrient scavenging in cancer., Nat Rev Cancer 18 619–633 doi: 10.1038/s41568-018-0048-x 30097614.

Fletcher K, Ulferts, R, Jacquin E, Veith T, Gammoh N, Arasteh JM, *et al.* (2018). The WD40 domain of ATG16L1 is required for its non-canonical role in lipidation of LC3 at single membranes. EMBO J 37, e97840.

Florey O, Gammoh N, Kim SE, Jiang X, Overholtzer M (2015). V-ATPase and osmotic imbalances activate endolysosomal LC3 lipidation. Autophagy 11, 88–99.

Florey O, Overholtzer M (2019). Macropinocytosis and autophagy crosstalk in nutrient scavenging. Philos Trans R Soc Lond B Biol Sci 374, 20180154.

Fujii M, Kawai K, Egami Y, Araki N (2013). Dissecting the roles of Rac1 activation and deactivation in macropinocytosis using microscopic photomanipulation. Sci Rep 3, 2385.

Gao Y, Liu Y, Hong L, Yang Z, Cai X, Chen X, *et al.* (2016). Golgi-associated LC3 lipidation requires V-ATPase in noncanonical autophagy. Cell Death Dis 7, e2330.

Gekle M, Freudinger R, Mildenberger S (2001). Inhibition of Na+-H+ exchanger-3 interferes with apical receptor-mediated endocytosis via vesicle fusion. J Physiol (Lond) 531, 619–629.

Gutierrez A, Pan Li, Groen RWJ, Baleydier F, Kentsis J, Marineau J, *et al.* (2014). Phenothiazines induce PP2A-mediated apoptosis in T cell acute lymphoblastic leukemia. J Clin Invest 124, 644–655.

Hernandez-Valladares M, Kim T, Kannan B, Tung A, Aguda AH, Larsson M, Cooper JA, Robinson RC (2010). Structural characterization of a capping protein interaction motif defines a family of actin filament regulators. Nat Struct Mol Biol 17, 497–503.

Hodakoski C, Hopkins BD, Zhang G, Su T, Cheng Z, Morris R, Rhee KY, Goncalves MD, Cantley LC (2019). Rac-mediated macropinocytosis of extracellular protein promotes glucose independence in non-small cell lung cancer. Cancers (Basel) 11, 37.

Hoeller O, Bolourani P, Clark J, Stephens LR, Hawkins PT, Weiner OD, Weeks G, Kay RR (2013). Two distinct functions for PI3-kinases in macropinocytosis. J Cell Sci 126, 4296–4307.

Inoue M, Enomoto M, Yoshimura M, Mizowaki T (2021). Pharmacological inhibition of sodium-calcium exchange activates NADPH oxidase and induces infection-independent NETotic cell death. Redox Biol 43, 101983.

Isom DG, Sridharan V, Baker R, Clement ST, Smalley DM, Dohlman HG (2013). Protons as second messenger regulators of G protein signaling. Mol Cell 51, 531–538.

Jacquin E, Leclerc-Mercier S, Judon C, Blanchard E, Fraitag S, Florey O (2017). Pharmacological modulators of autophagy activate a parallel noncanonical pathway driving unconventional LC3 lipidation. Autophagy 13, 854–867.

Jayashankar V, Edinger AL (2020). Macropinocytosis confers resistance to therapies targeting cancer anabolism. Nat Commun 11, 1121.

Jayashankar V, Finicle BT, Edinger AL (2018). Starving PTEN-deficient prostate cancer cells thrive under nutrient stress by scavenging corpses for their supper. Mol Cell Oncol 5, e1472060.

Jenkins EC, Debnath S, Gundry S, Gundry S, Uyar U, Fata JE (2012). Intracellular pH regulation by Na^+/H^+ exchanger-1 (NHE1) is required for growth factor-induced mammary branching morphogenesis. Dev Biol 365, 71–81.

Jin X, Zhou M, Chen S, Li D, Cao X, Liu B (2022). Effects of pH alterations on stress- and aging-induced protein phase separation. Cell Mol Life Sci 79, 380.

Kabayama H, Takeuchi M, Taniguchi M, Tokushige N, Kozaki S, Mizutani A, Nakamura T, Mikoshiba K (2011). Syntaxin 1B suppresses macropinocytosis and semaphorin 3A-induced growth cone collapse. J Neurosci 31, 7357–7364.

Kabeya Y, Mizushima N, Yamamoto A, Oshitani-Okamoto S, Ohsumi Y, Yoshimori T (2004). LC3, GABARAP and GATE16 localize to autophagosomal membrane depending on form-II formation. J Cell Sci 117, 2805–2812.

Kaizuka T, Morishita H, Hama Y, Tsukamoto S, Matsui T, Toyota Y, Kodama A, Ishihara T, Mizushima T, Mizushima N (2016). An autophagic flux probe that releases an internal control. Mol Cell 64, 835–849.

Kast DJ, Dominguez R (2017). The cytoskeleton-autophagy connection. Curr Biol 27, R318–R326.

Kim SM, Nguyen TT, Ravi A, Kubiniok P, Finicle BT, Jayashankar V, *et al.* (2018). PTEN deficiency and AMPK activation promote nutrient scavenging and anabolism in prostate cancer cells. Cancer Discov 8, 866–883.

Kitazawa S, Nishizawa S, Nakagawa H, Funata M, Nishimura K, Soga T, Hara T (2017). Cancer with low cathepsin D levels is susceptible to vacuolar (H+)-ATPase inhibition. Cancer Sci 108, 1185–1193.

Ko M, Quiñones-Hinojosa A, Rao R (2020). Emerging links between endosomal pH and cancer. Cancer Metastasis Rev 39, 519–534.

Koivusalo M, Welch C, Hayashi H, Scott CC, Kim M, Alexander T, Touret N, Hahn KM, Grinstein S (2010). Amiloride inhibits macropinocytosis by lowering submembranous pH and preventing Rac1 and Cdc42 signaling. J Cell Biol 188, 547–563.

Kozma SC, Bogaard ME, Buser K, Saurer SM, Bos JL, Groner B, Hynes NE (1987). The human c-Kirsten ras gene is activated by a novel mutation in codon 13 in the breast carcinoma cell line MDA-MB231. Nucleic Acids Res 15, 5963–5971.

Lee Y-K, Lee J-A (2016). Role of the mammalian ATG8/LC3 family in autophagy: differential and compensatory roles in the spatiotemporal regulation of autophagy. BMB Rep 49, 424–430.

Li Z-L, Zhang H-L, Huang Y, Huang J-H, Sun P, Zhou N-N, *et al.* (2020). Autophagy deficiency promotes triple-negative breast cancer resistance to T cell-mediated cytotoxicity by blocking tenascin-C degradation. Nat Commun 11, 3806.

Lin H-P, Singla B, Ahn W, Ghoshal P, Blahove M, Cherian-Shaw M, *et al.* (2022). Receptor-independent fluid-phase macropinocytosis promotes

arterial foam cell formation and atherosclerosis. Sci Transl Med 14, eadd2376.
Lin H-P, Singla B, Ghoshal P, Faulkner JL, Cherian-Shaw M, O'Connor PM, She J-X, Belin de Chantemele EJ, Csányi G (2018). Identification of novel macropinocytosis inhibitors using a rational screen of Food and Drug Administration-approved drugs. Br J Pharmacol 175, 3640–3655.
Liu Y, Luo X, Shan H, Fu Y, Gu Q, Zheng X, *et al*. (2019). Niclosamide triggers non-canonical LC3 lipidation. Cells 8, 248.
Lystad AH, Carlsson SR, de la Ballina LR, Kauffman KJ, Nag S, Yoshimori T, Melia TJ, Simonsen A (2019). Distinct functions of ATG16L1 isoforms in membrane binding and LC3B lipidation in autophagy-related processes. Nat Cell Biol 21, 372–383.
Lystad AH, Simonsen A (2019). Mechanisms and pathophysiological roles of the ATG8 conjugation machinery. Cells 8, 973.
Masereel B (2003). An overview of inhibitors of Na+/H+ exchanger. Eur J Med Chem 38, 547–554.
Maxson ME, Sarantis H, Volchuk A, Brumell JH, Grinstein S (2021). Rab5 regulates macropinocytosis by recruiting the inositol 5-phosphatases OCRL and Inpp5b that hydrolyse PtdIns(4,5)P2. J Cell Sci 134, jcs252411.
Meerbrey KL, Hu G, Kessler JD, Roarty K, Li MZ, Fang JE, *et al*. (2011). The pINDUCER lentiviral toolkit for inducible RNA interference in vitro and in vivo. Proc Natl Acad Sci U S A 108, 3665–3670.
Miki H, Suetsugu S, Takenawa T (1998). WAVE, a novel WASP-family protein involved in actin reorganization induced by Rac. EMBO J 17, 6932–6941.
Mizushima N, Yoshimori T (2007). How to interpret LC3 immunoblotting. Autophagy 3, 542–545.
Mylvaganam S, Freeman SA, Grinstein S (2021). The cytoskeleton in phagocytosis and macropinocytosis. Curr Biol 31, R619–R632.
Nonnenmacher ME, Cintrat J-C, Gillet D, Weber T (2015). Syntaxin 5-dependent retrograde transport to the trans-Golgi network is required for adeno-associated virus transduction. J Virol 89, 1673–1687.
Okreglak V, Ling R, Ingaramo M, Thayer NH, Millett-Sikking A, Gottschling DE (2023). Cell cycle-linked vacuolar pH dynamics regulate amino acid homeostasis and cell growth. Nat Metab 5, 1803–1819.
Orij R, Brul S, Smits GJ (2011). Intracellular pH is a tightly controlled signal in yeast. Biochim Biophys Acta 1810, 933–944.
Palm W (2022). Signaling pathways that regulate macropinocytosis in mammalian cells. Subcell Biochem 98, 143–167.
Palm W, Araki J, King B, DeMatteo RG, Thompson CB (2017). Critical role for PI3-kinase in regulating the use of proteins as an amino acid source. Proc Natl Acad Sci U S A 114, E8628–E8636.
Qiu Z, Liu W, Zhu Q, Ke K, Zhu Q, Jin W, *et al*. (2022). The role and therapeutic potential of macropinocytosis in cancer. Front Pharmacol 13, 919819.
Ramirez C, Hauser AD, Vucic EA, Bar-Sagi D (2019). Plasma membrane V-ATPase controls oncogenic RAS-induced macropinocytosis. Nature 576, 477–481.
Redelman-Sidi G, Binyamin A, Gaeta I, Palm W, Thompson CB, Romesser PB, *et al*. (2018). The canonical wnt pathway drives macropinocytosis in cancer. Cancer Res 78, 4658–4670.
Reid SE, Kolapalli SP, Nielsen TM, Frankel LB (2022). Canonical and non-canonical roles for ATG8 proteins in autophagy and beyond. Front Mol Biosci 9, 1074701.
Ridley AJ, Paterson HF, Johnston CL, Diekmann D, Hall A (1992). The small GTP-binding protein rac regulates growth factor-induced membrane ruffling. Cell 70, 401–410.
Rolver MG, Elingaard-Larsen LO, Andersen AP, Counillon L, Pedersen SF (2020). Pyrazine ring-based Na+/H+ exchanger (NHE) inhibitors potently inhibit cancer cell growth in 3D culture independent of NHE1. Sci Rep 10, 5800.
Romero-Moreno R, Czowski BJ, Harris L, Kuehn JF, White KA (2024). Intracellular pH differentially regulates transcription of metabolic and signaling pathways in normal epithelial cells. J Biol Chem 300, 107658.
Sanjana NE, Shalem O, Zhang F (2014). Improved vectors and genome-wide libraries for CRISPR screening. Nat Methods 11, 783–784.
Sedlyarov V, Eichner R, Girardi E, Essletzbichler P, Goldmann U, Nunes-Hasler P, *et al*. (2018). The bicarbonate transporter SLC4A7 plays a key role in macrophage phagosome acidification. Cell Host Microbe 23, 766–774.e5.
Slepkov ER, Rainey JK, Sykes BD, Fliegel L (2007). Structural and functional analysis of the Na+/H+ exchanger. Biochem J 401, 623–633.
Spear JS, White KA (2023). Single-cell intracellular pH dynamics regulate the cell cycle by timing the G1 exit and G2 transition. J Cell Sci 136, jcs260458.
Steffan JJ, Snider JL, Skalli O, Welbourne T, Cardelli JA (2009). Na+/H+ exchangers and RhoA regulate acidic extracellular pH-induced lysosome trafficking in prostate cancer cells. Traffic 10, 737–753.
Stock C, Gassner B, Hauck CR, Arnold H, Mally S, Eble JA, Dieterich P, Schwab A (2005). Migration of human melanoma cells depends on extracellular pH and Na+/H+ exchange. J Physiol (Lond) 567, 225–238.
Stock C, Pedersen SF (2017). Roles of pH and the Na+/H+ exchanger NHE1 in cancer: From cell biology and animal models to an emerging translational perspective? Semin Cancer Biol 43, 5–16.
Stockinger W, Zhang SC, Trivedi V, Jarzylo LA, Shieh EC, Lane WS, Castoreno AB, Nohturfft A (2006). Differential requirements for actin polymerization, calmodulin, and Ca2+ define distinct stages of lysosome/phagosome targeting. Mol Biol Cell 17, 1697–1710.
Su H, Yang F, Fu R, Li X, French R, Mose E, *et al*. (2021). Cancer cells escape autophagy inhibition via NRF2-induced macropinocytosis. Cancer Cell 39, 678–693.e11.
Swanson JA (1989). Phorbol esters stimulate macropinocytosis and solute flow through macrophages. J Cell Sci 94 (Pt 1), 135–142.
Tajiri H, Uruno T, Shirai T, Takaya D, Matsunaga S, Setoyama D, *et al*. (2017). Targeting Ras-driven cancer cell survival and invasion through selective inhibition of DOCK1. Cell Rep 19, 969–980.
Tanida I, Ueno T, Kominami E (2008). LC3 and autophagy. Methods Mol Biol 445, 77–88.
Tisdale EJ, Shisheva A, Artalejo CR (2014). Overexpression of atypical protein kinase C in HeLa cells facilitates macropinocytosis via Src activation. Cell Signal 26, 1235–1242.
Tsherniak A, Vazquez F, Montgomery PG, Weir BA, Kryukov G, Cowley GS, *et al*. (2017). Defining a cancer dependency map. Cell 170, 564–576.e16.
Uphoff CC, Drexler HG (2014). Detection of Mycoplasma contamination in cell cultures. Curr Protoc Mol Biol 106, 28.4.1–28.4.14.
Veltman DM, Williams TD, Bloomfield G, Chen B-C, Betzig E, Insall RH, Kay RR (2016). A plasma membrane template for macropinocytic cups. Elife 5, e20085.
Wang Y *et al*. (2016). Dual T cell- and B cell-intrinsic deficiency in humans with biallelic RLTPR mutations. J Exp Med 213, 2413–2435.
Wang Y, Ramos M, Jefferson M, Zhang W, Beraza N, Carding S, Powell PP, Stewart JP, Mayer U, Wileman T (2022). Control of infection by LC3-associated phagocytosis, CASM, and detection of raised vacuolar pH by the V-ATPase-ATG16L1 axis. Sci Adv 8, eabn3298.
West MA, Bretscher MS, Watts C (1989). Distinct endocytotic pathways in epidermal growth factor-stimulated human carcinoma A431 cells. J Cell Biol 109, 2731–2739.
West MA, Prescott AR, Eskelinen EL, Ridley AJ, Watts C (2000). Rac is required for constitutive macropinocytosis by dendritic cells but does not control its downregulation. Curr Biol 10, 839–848.
Yamamoto K, Venida A, Yano J, Biancur DE, Kakiuchi M, Gupta S, *et al*. (2020). Autophagy promotes immune evasion of pancreatic cancer by degrading MHC-I. Nature 581, 100–105.
Zeng H, Park JW, Guo M, Lin G, Crandall L, Compton T, Wang X, Li X-J, Chen F-P, Xu R-H (2009). Lack of ABCG2 expression and side population properties in human pluripotent stem cells. Stem Cells 27, 2435–2445.
Zhang P, Liu X, Li H, Chen Z, Yao X, Jin J, Ma X (2017). TRPC5-induced autophagy promotes drug resistance in breast carcinoma via CaMKKβ/AMPKα/mTOR pathway. Sci Rep 7, 3158.
Zhang Y, Recouvreux MV, Jung M, Galenkamp KMO, Li Y, Zagnitko O, Scott DA, Lowy AM, Commisso C (2021). Macropinocytosis in cancer-associated fibroblasts is dependent on CaMKK2/ARHGEF2 signaling and functions to support tumor and stromal cell fitness. Cancer Discov 11, 1808–1825.
Zwolak A, Yang C, Feeser EA, Ostap EM, Svitkina T, Dominguez R (2013). CARMIL leading edge localization depends on a non-canonical PH domain and dimerization. Nat Commun 4, 2523.